DEUTSCHES ELEKTRONEN – SYNCHROTRON

DESY 92-002
FTUAM-EP-92-01
January 1992

Gluon Density Determination from Open Charm Events at HERA

R. van Woudenberg
NIKHEF-H, Amsterdam, The Netherlands

F. Ould-Saada
II. Institut für Experimentalphysik, Universität Hamburg

F. Barreiro, J. del Peso, J. F. de Trocóniz
Universidad Autónoma de Madrid, Spain

Y. Eisenberg, C. Glasman, U. Karshon, A. Montag
Weizmann Institute for Physics, Rehovot, Israel

S. Egli
Universität Zürich, Switzerland

ISSN 0418-9833

NOTKESTRASSE 85 · D-2000 HAMBURG 52

To be sure that your preprints are promptly included in the
HIGH ENERGY PHYSICS INDEX,
send them to the following (if possible by air mail):

DESY Bibliothek Notkestraße 85 W-2000 Hamburg 52 Germany	DESY-IfH Bibliothek Platanenallee 6 O-1615 Zeuthen Germany

DESY 92-002
FTUAM-EP-92-01
January 1992

ISSN 0418-9833

Gluon density determination from open charm events at HERA[1]

R. van Woudenberg

NIKHEF-H, Amsterdam, The Netherlands

F. Ould-Saada

II Inst. f. Exp. Phys. der Universität Hamburg
Hamburg, Fed. Rep. Germany

F. Barreiro, J. del Peso, J.F. de Trocóniz

Universidad Autónoma de Madrid, Madrid, Spain [2]

Y. Eisenberg, C. Glasman, U. Karshon, A. Montag

Weizmann Institute for Physics, Rehovot, Israel

S. Egli

Universität Zürich, Zürich, Switzerland

[1]To be published in the Proceedings of the DESY Workshop Physics at HERA, Hamburg, FRG(1991).
[2]Supported by CICYT.

Abstract

We study some prospects of measuring the gluon density in the proton using charm events at HERA for the ep center of mass energy $\sqrt{s} = 314\ GeV$. We invoke the QCD-improved boson-gluon fusion model and find the following cross-section: $\sigma(ep \rightarrow ec\bar{c}X) \simeq O(0.6\ \mu b)$. This cross-section would provide $O(10^8)$ events/year, for an integrated luminosity of 100 pb^{-1}. We have investigated two traditional methods for tagging of charm, namely, $D^{*\pm}$ reconstruction using the process $D^{*\pm} \rightarrow D^0\pi^\pm \rightarrow (K^\mp\pi^\pm)\pi^\pm$, and dileptonic decays of charmed hadrons ($c\bar{c} \rightarrow l^+l^-X$). The inclusive cross-sections after full detector simulation are 10^3 pb and 10^2 pb, respectively. In both cases the background was strongly reduced. By using these events, the gluon distribution in the proton can be measured in the range $10^{-3} \leq x_g \leq 10^{-1}$. We conclude that an adequate discrimination among the present theoretical parametrizations can be achieved at HERA.

1 Introduction

The study of heavy quark production at HERA will provide important testing grounds for the standard model [1]. For a designed yearly luminosity of 100 pb^{-1} one expects of the order of 10^8 (10^6) $c\bar{c}$ pairs (resp. $b\bar{b}$ pairs) to be produced at HERA.

In particular the charm (bottom) production cross-section through the boson-gluon mechanism is two orders of magnitude larger than (resp. comparable to) those at LEP. This will enable HERA experiments to undertake some precison measurements both in the charm and bottom sectors, as already discussed in [1]. In this paper, we would like to turn our attention to the possibility of extracting the gluon density in the proton.

Measurements of the parton densities in the proton are not only essential to deepen our understanding of the nucleon structure or to test the QCD evolution equations, but also crucial to understand the physics at present ($Sp\bar{p}S$, Tevatron) and future (LHC, SSC) hadron colliders.

Fixed target deep inelastic experiments performed in the past, either with lepton or photon beams, have provided valuable direct information about the valence and sea quark distributions. The former are known to peak at around $\frac{1}{3}$ as expected in the naive quark parton model, while vanishing at both ends of the spectrum. The latter are known to fall off very sharply, being negligible for x values larger than 0.30.

Although it is well known that gluons should carry approximately 50% of the proton momentum, the gluon density is poorly measured. This has to do with the fact that previous fixed target muon or neutrino experiments were limited to measurements of the proton structure functions in the true deep inelastic limit, i.e. $Q^2 \geq 4\ GeV^2$, for x values essentially above 0.1.

Traditionally the gluon density has been extracted using the following two methods:

- measuring the scaling violation effects present in the proton structure functions F_2 [2] or F_3 [3] and solving the QCD evolution equations.
- measuring the longitudinal structure function which is defined as:

$$F_L(x,Q^2) = F_2(x,Q^2) - 2xF_1(x,Q^2) \tag{1}$$

  thus giving information on the deviations from the Callan-Gross relation valid in the quark parton model i.e. assuming that the lepton scatters off spin $\frac{1}{2}$ fermions inside the proton. The longitudinal structure function relates to the gluon density through an expression similar in structure to the one for the Q^2 variation of F_2.

The usual procedure was to parametrise the gluon density at a fixed Q_0^2 to an expression of the form

$$x_g.G(x_g) = A_g \cdot (1 - x_g)^{\eta_g} \tag{2}$$

and fit one of the previous evolution equations to the structure function data. Free parameters in the fits are Λ_{QCD} as well as η_g. This indirect procedure has clear limitations of a theoretical as well as an experimental nature, namely:

- there is a strong correlation between Λ_{QCD} and the parameters entering into the gluon density parametrization.

- it is obviously insensitive to x_g values below those at which the structure function measurements have been performed.

Thus, the gluon density for x values smaller than $O(0.1)$ is not yet measured, and for values above this limit the uncertainties are much larger than those affecting the valence and sea quark distributions.

Heavy quark pair production offers a possibility to measure the gluon density directly. Several approaches have been devised to get a glance at the gluon density using quark-pair produced events. They range from :

- simple methods where one measures inclusive distributions which are able to discriminate among current parametrizations.
- more elaborate ones where one attempts reconstructing the kinematical variables x_g and $\hat{s}$ and subsequently unfolding of the gluon density from the data.

The aim of this paper is to illustrate how these methods work in a study case: charm production. In section 2, the charm cross-sections in leading order, their ambiguities and higher order corrections are discussed. Section 3 is devoted to charm tagging schemes, namely D^* reconstruction and semi-leptonic decays. Inclusive distributions presented in section 4 are used to discriminate among current parametrizations of the gluon density. We discuss direct methods to reconstruct the fractional momentum of the proton carried by the gluons, x_g, as well as the center of mass energy of the boson-gluon interaction, $\hat{s}$, in section 5. Here a number of possibilities are considered, namely:

- two-jet production.
- inclusive and semi-inclusive D^* production.
- dileptonic final states.

The pros and cons of these various alternatives, the precision and range of applicability for x_g and $\hat{s}$ reconstruction, are discussed. In section 6 unfolding of the gluon density function $G(x_g,\mu^2)$ is performed and some sources of systematic errors are studied. Section 7 is left for a summary and conclusions.

We would like to finally point out that the interest in heavy quark physics at HERA is by no means exhausted by the determination of the gluon density using charm events, the subject matter of this paper. Therefore we would like to urge the interested reader to consult the reports written for this workshop by other subgroups.

2 Charm production at HERA

2.1 Leading order results and experimental characteristics

Since the Quark-Parton model contribution is negligible, $O(10\ pb)$ at HERA [1], in high energy ep collisions the leading order contribution to charm production is due to the boson-gluon fusion (BGF) mechanism shown in Figure 1:

$$\gamma/Z^0 + g \rightarrow c + \bar{c} \tag{3}$$

It occurs as $O(\alpha^2\alpha_S)$ subprocess in the corresponding ep scattering:

$$e + p \rightarrow e + c + \bar{c} + X \tag{4}$$

Boson-gluon fusion is the lowest order result in Quantum Chromodynamics (QCD) up to corrections which are suppressed by powers of the heavy quark mass [4]. This process uses the gluon density in a proton as input. Conversely, a measurement of the charm electroproduction cross-sections yields crucial information on the gluon distribution function [5].

The invariant matrix elements squared and the cross-section for this process have been available in the literature for some time [6]. They take into account the heavy quark mass, the full electroweak structure of the reaction and arbitrary longitudinal polarization of the incoming electron or positron. For values of the quark mass $m_c = 1.5\ GeV$, QCD scale $\Lambda_{QCD} = 0.2\ GeV$, number of active flavours in running α_S $n_f = 3$, mass scales $\mu_R = \mu_F = \sqrt{\hat{s}}$ and gluon density parametrization EHLQ (set 1) [7] it was found that $\sigma(ep \rightarrow ec\bar{c}X) \sim 0.5\ \mu b$ at HERA energies ($\sqrt{s} = 314\ GeV$). This number is, for instance, two orders of magnitude larger than charm production at LEP-I. So, for a nominal integrated luminosity of 100 pb^{-1} per year delivering 10^8 charmed particles, HERA could well be considered as a charm factory.

The phenomenological consequences of the lowest order formulae can be summarized as follows [8]:

- The cross-section peaks at very low Q^2: $Q^2_{min} \sim 10^{-15}\ GeV^2$ and $d\sigma/dQ^2 \sim Q^{-2}$. It is mainly a photoproduction process. The scattered electron typically disappears into the beam pipe.
- The average transverse momentum of the charmed quark or antiquark is of the order of its mass and the $p_\perp$-distribution falls rapidly to zero for larger values.
- The rapidity distribution is rather central in spite of the HERA laboratory frame boost. The rapidity difference between the produced quark and antiquark is $O(1)$.

2.2 QCD radiative corrections and their uncertainties

Investigations of the QCD corrections to heavy flavour photoproduction have been undertaken, up to now, by taking into account:

- $O(\alpha\alpha_S{}^2)$ point-like contribution with cuts to avoid the singular regions in phase space [1,9].
- Resolved-photon component to b-quark production [1,9,10,11].
- The full $O(\alpha\alpha_S{}^2)$ cross-section calculation [12,13].

The electroproduction case can be obtained in the Weizsäcker-Williams approximation.

The basic subprocesses leading to the point-like component of the NLO are:

$$\gamma + g \rightarrow c + \bar{c} + g \tag{5}$$

$$\gamma + q(\bar{q}) \rightarrow c + \bar{c} + q(\bar{q}) \tag{6}$$

including virtual corrections to the Born reaction (3). Ellis and Nason [12] used their results, obtained in the $\overline{\rm MS}$ factorization scheme, to fit low energy fixed target photoproduction

data. They conclude that it can be achieved for $m_c = 1.5 \pm 0.3\ GeV$. Smith and van Neerven [13] went one step beyond and calculated corrections for single particle inclusive differential distributions at HERA. The calculation was performed in both the $\overline{\rm MS}$ and DIS mass factorization schemes (the difference being small). They checked that they reproduce the formulae and the cross-section of [12].

These corrections turn to be important at:

- Threshold, more specifically, $\hat{s} \leq 11\ GeV^2$.
- Large energies: $\hat{s} \geq 200\ GeV^2$. In this limit, $\rho \equiv 4m_c^2/\hat{s} \rightarrow 0$, the cross-section shows a plateau behaviour with the dominant configuration being described as charm excitation inside the photon *à la* Bethe-Heitler. Large logarithms like $(\alpha_S \log(4m_Q^2/s))^n$ are expected to appear in the following perturbative terms. These contributions can be resummed in all orders [14,15].

The $O(\alpha^2\alpha_S{}^2)$ resolved-photon charm production at HERA proceeds via two reactions:

$$g + g \rightarrow c + \bar{c} \tag{7}$$

$$q + \bar{q} \rightarrow c + \bar{c} \tag{8}$$

This cross-section has turned out to represent only $15 - 40\%$ of the direct channel, depending on the assumed densities inside the photon. Moreover, the gluon-gluon scattering is dominant, the $q - \bar{q}$ component being suppressed by an additional order of magnitude [16].

The uncertainties on the QCD prediction are large. The first ambiguity is whether the QCD-corrected boson-gluon fusion model can describe charm production at all. The mass of the charmed quark might not be big enough compared to the QCD scale Λ_{QCD} and, then, effects nominally suppressed by powers of m_c would be important [4]. Although there is a general belief that m_c is on the edge of the region where perturbative QCD is applicable, it is fair to say that QCD provides an adequate account of charm photoproduction at present experiments using $m_c \sim 1.5\ GeV$ [12,17,18,19,20].

A related uncertainty is the value of the heavy quark mass. The dependence of the cross-section on the mass of the charmed quark is important and is mostly due to the dependence on variables strongly peaking at threshold. For example, $Q^2_{min} \propto m_c^4$ and $x_g^{min} \propto m_c^2$. Allowing an error of $\Delta m_c = \pm 0.3\ GeV$, the relative change in the cross- section propagates to $\Delta\sigma/\sigma \sim^{-0.4}_{+0.9}$ [1,12].

Next, we consider the lack of knowledge in the mass renormalization (μ_R) and factorization (μ_F) scales. The scales are only constrained a priori to be of the order of the heavy quark mass because this is at least the virtuality of the internal fermionic line at the lowest order graphs [4]. In [12], the quoted errors were calculated allowing for a variation of μ in the range $\frac{1}{2}m_c < \mu \equiv \mu_R = \mu_F < 2m_c$. After inclusion of $O(\alpha_S)$ corrections no large improvement in the scale dependence is seen. This is mostly due to to the fact that $\alpha(\mu_R)$ is still large, the dependence in μ_F being smaller [13].

Another uncertainty is due to Λ_{QCD}, which influences the evolution properties of the gluon density and α_S. The authors of [12] assumed in their calculation $\Lambda_4 = 260 \pm 100 MeV$. The corresponding error in the cross-section was added in quadrature to those coming from the μ-dependence to obtain their final numbers: $\Delta\sigma/\sigma \sim 30\%$.

Last but not least, considerable uncertainties pertain to the gluon density, which can be probed at HERA using charm events up to $x_g = 10^{-4}$. In these small x_g regions the

form of the gluon distribution function is still unmeasured. There are good arguments to expect that the gluon density at small x_g would show a certain shadowing behaviour due to QCD non-linear effects [21]. We have, however, used the classical approach in the evolution of the parton densities [22,23]. Even so, the spread in the low x_g behaviour exhibited by present parametrizations is large. In fact, a parametrization with $x_g.G(x_g) \sim 1/\sqrt{x_g}$ at small x_g increases the charm cross-section by a factor of two as compared to other predictions of conventional type (e.g.[7]) [1]. As we will see, HERA will have the chance to discriminate among these alternatives by using, for instance, open charm events.

With all this into consideration, the full NLO cross-section result for $m_c = 1.5\ GeV$ at HERA energies given in [12] is:

$$\sigma(ep \to ec\bar{c}X) = 0.68\ ^{+0.26}_{-0.18}\ \mu b \tag{9}$$

2.3 Gluon density reconstruction

The aim of this paper is to extract the leading order gluon density by explicit reconstruction of x_g, the momentum fraction of the proton carried by the gluon. This means that we are dealing with a very definite kinematics: we will consider charm production as a $2 \to 2$ process. Thus, we will always assume in this paper that the connection between the measured physical cross-sections and the gluon function we want to extract is given by the partonic hard scattering matrix elements evaluated at the lowest order boson-gluon fusion times an experimental factor depending on the particular channel we are looking at. This factor includes fragmentation properties, branching ratios and detection acceptances and resolutions. Symbolically:

$$\sigma = \int dx_g\ G(x_g,\mu^2)\ \hat{\sigma}_{LO}(\hat{s},\mu^2,m_c^2)\ A_{exp} \tag{10}$$

On the other hand we have seen in the last section that the NLO corrections are pretty large in some phase space regions. Furthermore, there exists the possibility that our familiar kinematics is completely distorted by the $2 \to 3$ processes, such as $\gamma g \to c\bar{c}g$. We have then sketched a number of sensible requirements to get rid of all these unwanted contributions. But, of course, definitive conclusions could only be reached once the full matrix elements are implemented in a generator program. This has not yet been achieved.

We would like to remark that we will not really discuss the absolute normalization since only the shape of the gluon function is going to be reconstructed. Furthemore, it has been shown [13] that the shape of the one-particle inclusive $p_\perp$ and rapidity distributions remains mostly unchanged after including the NLO QCD adjustments.

The large corrections at threshold are easily suppressed by any realistic experimental trigger requirement. For example, typical visibility conditions in our simulations lead to an implicit demand on the $p_\perp$ of the produced quark $p_\perp(c) \geq 2\ GeV$.

In the limit $\rho \to 0$, the leading topological configuration can be considered as a charm quark in the photon scattered off a light quark or gluon inside the proton to produce one charmed and one light jet. The second heavy quark in the photon wave function would disappear into the beam pipe at very large, negative rapidities. This kind of $2 \to 2$ events could be suppressed e.g. by methods tagging on both c and $\bar{c}$.

As already discussed above, the resolved-photon contribution is not large. Theoretical studies in [13] reveal that this component is completely dominated by the point-like cross-section in the one-particle inclusive $p_\perp$ and rapidity distributions. Second, it is mainly gluon-

initiated. So, in principle, one would be allowed to add it to the signal as shown in [5]. In [10], it is further discussed how choosing the rapidity of one of the produced heavy quark or antiquark allows to remove all resolved contributions without losses in the x_g-range of sensitivity. Another possibility would be to tag on the spectator jet from the photon but, since we do not have experimental information yet, it is difficult to make any quantitative statement.

On the other hand, the light two-jet production at HERA will be dominated by the anomalous-photon component. It has been included in a large part of the following analysis in order to compute the background. We would like to point out that the acceptance of the trigger cuts is large even for events in the region where perturbative predictions begin to collapse. Probably one should wait for data to obtain reliable background estimates.

We have also included effects of soft partonic initial and final state radiation in a parton cascade approach. We have used a simulation based on the leading-log Altarelli-Parisi splitting functions as implemented in the program PYTHIA [24,25]. This leads to a better description of the internal structure of jets and also gives rise to multijet events. Events with large accumulated radiative activity have been shown to be very much suppressed when requiring a back-to-back two jet pattern in the transverse plane [26].

3 Tagging charm events at HERA

3.1 D^* reconstruction

In this section we briefly describe the D^* tagging method. For more details see [27,28,29]. The results were obtained using the simulations of the H1 and ZEUS detectors which take into account energy loss and the resolution of the apparatus. The momentum resolution of the tracking detectors is $\frac{\sigma_p}{p^2} \sim 0.3\%/GeV$.

The reconstruction of charged D^* mesons is a powerful method of tagging the charmed quark, due to the very tight kinematical constraints on the decay

$$D^{*+} \to D^0\pi^+, \quad D^{*-} \to \bar{D}^0\pi^- \tag{11}$$

where the single pion has a kinetic energy (momentum) of 5.8 MeV (resp. 40 MeV/c) in the $D^{*\pm}$ rest frame. Consequently, the mass difference

$$\Delta M = M(D^0\pi^+) - M(D^0) \tag{12}$$

can be measured more accurately than the $D^{*\pm}$ mass itself [30]. In reconstructing the D^0 through the $K^-\pi^+$ decay mode[3], which has a branching ratio of $O(4\%)$, charged tracks within a certain angular range ($10^\circ \leq \theta \leq 165^\circ$ for H1 and $|\eta| \leq 3$ for ZEUS) with momenta $p > 0.6\ GeV/c$ were combined. No particle identification was used and each track was considered in turn to be a kaon or a pion. The combination was accepted as a possible candidate D^0 if the $K^-\pi^+$ invariant mass lies in the range $1.82 < M(K^-\pi^+) < 1.91\ GeV$.

To form a $D^{*\pm}$, these D^0 candidates were combined with an additional charged track, assumed to be a pion, with a momentum cut $0.15 < p(\pi) < 5.0\ GeV/c$. The kaon and the additional pion were required to have opposite charges. A final state $(K^+\pi^-)\pi^+$, where the

[3] Other channels like $D^0 \to K^-\pi^+\pi^-\pi^+$ ($\sim 10\%$ BR) and the Cabibbo suppressed decays $D^0 \to K^+K^-$ ($\sim 0.5\%$ BR) and $D^0 \to \pi^+\pi^-$ ($\sim 0.1\%$ BR) are under study.

kaon and the additional pion have the same charge, can come from two interesting sources: $D-\bar{D}$ mixing ($D^0 \to \bar{D}^0 \to K^+\pi^-$) or the doubly Cabibbo suppressed decay ($D^0 \to K^+\pi^-$). These processes could be studied using a vertex detector. Figure 5 shows the invariant mass distribution $M(K^-\pi^+)$. $c\bar{c}$ events (a) present a peak at the D^0 mass, 1865 MeV, while background events (b) do not. The D^0 mass resolution is $O(20\ MeV/c^2)$. Figure 6(a) shows the resulting distribution of the mass difference $\Delta M = M(K^-\pi^+\pi^+) - M(K^-\pi^+)$ for $c\bar{c}$ and background events (mainly from light quarks) [4]. The event generator PYTHIA [25], including initial state gluon radiation and both direct- and resolved-photon contributions (for heavy and light quark production) was used. We assumed branching ratios $P(c\bar{c} \to D^*X) = 53\%$, $\mathrm{BR}(D^{*+} \to D^0\pi^+) = 67\%$ [31] and $\mathrm{BR}(D^0 \to K^-\pi^+) = 4\%$. The tagging efficiency (including trigger[5]) is of the order of 10% (5% in the central tracker). With an integrated luminosity of $\int L.dt = 100\ \mathrm{pb}^{-1}$ per year, $O(10^5)$ $D^{*\pm}$ can be reconstructed annually. The signal-to-background ratio is of the order of 2 : 1. Additional cuts can be used to further reduce the light quark background:

- due to the hard charm quark fragmentation function, a cut on the ratio $x(D^*) = \frac{p(D^*)}{p(jet)}$ greater than 0.5 reduces the light quark contribution, while keeping most of the D^* events. Note that in this case jet reconstruction is necessary [29].
- the distribution of the cosine of the D^0 decay angle, the angle between the kaon and the D^0 direction of flight computed in the D^0 rest frame, is flat for signal events while it is peaked around ± 1 for faked background events.

The signal-to-background ratio can be further improved by requiring flavour separation via neural networks, K/π separation using dE/dx measurement and vertex detection [32,33] (Figure 6(b)).

3.2 Leptonic charm decays

In this section we shortly review the potential of HERA detectors to tag open $c\bar{c}$ events from their dileptonic decays. The interested reader should consult [34] for a detailed discussion. The utility of leptons as a tag for charmed hadrons at HERA was already considered in [1]. The branching ratio has been recently measured by ARGUS to be $\mathrm{BR}(c \to sl\nu) \simeq 20\%$ [35]. So, we expect a cross-section of $O(20\ nb)$ for dileptonic charmed events at HERA. The leptons from charm decays are mainly inside jets and have small energies. The average lepton energy is largest in the forward region and smallest in the central one.

Electron identification is based on calorimetric criteria, dE/dx losses in the tracking devices (CTD), transition radiation (TRD) and, in the case of ZEUS, a plane of silicon diodes in the rear region. The main background is, in fact, due to hadron misidentification in the detector. In Table 1 we show a number of kinematic and topological cuts useful to suppress the background. The strictest of them is the track transverse momentum requirement, $p_\perp \geq 0.8\ GeV$. This cut is, however, very useful in removing the background due to the

[4] The expected two-jet light quark cross-section, dominated by resolved photon contributions ($\sim 90\%$), represents the main source of background to heavy flavour production. This cross-section strongly depends on the cut applied on the transverse momentum of the light quark $p_\perp^{min}$. It is of the order of 1.2 mb for $p_\perp^{min} = 3\ GeV/c$. For $p_\perp^{min} = 2\ GeV/c$ (resp. 1 GeV/c) the cross-section increases by a factor of 4 (resp. 35). It is not yet clear whether QCD calculations are reliable for low transverse momenta (of the order of 1 GeV/c).

[5] The trigger efficiency is of the order of 40% for $c\bar{c}$ events

Cut	$\sigma(c\bar{c})$ [pb]
$\mathrm{BR}(c\bar{c} \to e^+e^-)$	5000.0
$\delta \leq 0.55$	4800.0
$\theta_{BP} = 0.1\ rad$	3000.0
$p_\perp(e^\pm) \geq 0.8 GeV$	70.0
$0.8 \leq E_{EMC}/P \leq 1.2$	45.0
TRD—dE/dx—Si	36.0
$\sum E_\perp \geq 6\ GeV$	32.0
$m(e^+e^-) \geq 1.5\ GeV$	32.0

Table 1: Cuts for selection of $c\bar{c} \to e^+e^-X$ events and remaining cross-sections.

progressive hardness of the quark $p_\perp$-spectrum and fragmentation function with its mass (see Figure 2). Moreover, to require a larger $p_\perp$ will oblige the electron to better remember the line of flight of its parent quark. For example, we find that our cut implies $p_\perp(c) \geq 2\ GeV$. That will finally improve the quality of the gluon fraction reconstruction. Also after this cut, the mean electron energy lies in the maximum of the sensitivity of our dE/dx and transition radiation devices.

The variable δ is defined in the following way:

$$\delta = \sum_{i=1}^{N_p} \frac{E_i - P_{Li}}{2E_e} \tag{13}$$

where N_p is the total number of particles detected and E_e is the nominal energy of the electron beam, which is assumed to have $P_L < 0$. Because of the energy-momentum conservation, if all the final state particles were detected, $\delta = 1$. In case the scattered electron is not observed, δ is just the variable used in the Jacquet-Blondel method to reconstruct y from the hadronic system. The cut $\delta < 0.55$ eliminates most of the events with a detected scattered electron (5%). Furthermore, this method of y-reconstruction is stable against QED-radiative events.

To identify a charged track as an electron with the calorimeter, the quantity E_{EMC}/P is used, where P is the momentum of the track measured in the CTD and E_{EMC} is the energy deposited in the appropriate electromagnetic section of the calorimeter. The differential cross-sections as function of E_{EMC}/P are displayed in Figure 3. The shaded histogram corresponds to electrons and the open one to hadrons. Ideally, a distribution centered at $E_{EMC}/P = 1$ is expected for electrons with spread $\sim O(10\%)$ from the energy resolution of the calorimeter and the momentum resolution of the CTD. One can observe a large difference between the hadron and the electron distributions, which allows to eliminate a large part of the hadronic background. For example, the cut $0.8 < E_{EMC}/P < 1.2$ rejects around 98% of the single hadrons keeping an electron efficiency higher than 80%. For dileptonic events this factor should be squared.

We have calculated the remaining cross-sections after cuts for two sets of gluon parametrizations. We have obtained 35 pb (39) for $c\bar{c} \to e^+e^-X$ events using Morfin-Tung set B1 (B2 respectively) [36]. There is also a contribution from $b\bar{b} \to e^+e^-X$ events of 17 pb. The background from misidentified hadrons amounts to 6 pb, where only point-like photon contributions have been considered. The average $\sqrt{\hat{s}}$ is about 11 GeV (14) for charm (beauty

respectively) tagged events. We have not tried further charm/bottom separation. Hence, we will combine both samples in the forthcoming analysis.

Muon identification was performed by using the instrumented iron which is equipped with limited streamer tubes in the case of H1 [27]. The geometrical efficiency (averaged in ϕ and sampled in 50 θ-bins) was estimated with the help of a full simulation program. At least 3 wire planes and 1 strip plane were required. A θ-dependent momentum cut of the order of $1.5 - 2\ GeV/c$ was demanded to be confident that the muon reaches the instrumented iron. The main source of background comes from K and π decays into μ in the central detector [37].

4 Inclusive distributions.

Inclusive distributions like, for instance, the rapidity or the $p_\perp$ of the produced D^*, are clearly sensitive to the gluon density. With the EHLQ parametrization it was already shown in [1] that approximately one third of the charmed mesons are produced in the forward, one third in the central and the remaining third in the backward region. Choosing a softer (harder) gluon density would result in more (less) charmed mesons being produced in the rear region. Thus, a measurement of the ratio $\frac{\sigma^{FW}(D^*)}{\sigma^{BW}(D^*)}$ i.e. of the ratio of D^*'s produced in the forward and backward hemispheres is sensitive to the gluon density.

This fast analysis method can be applied to discriminate among current parametrizations of the gluon density. To illustrate this point we show in Figure 4(a) the D^* rapidity distributions obtained with two sets of parametrizations of the gluon density [36] namely sets B1 and B2 from Morfin and Tung. The former gives rise to a gluon density which flattens off at $x_g \leq 10^{-2}$, a feature also exhibited by the EHLQ parametrization, while the latter shows a steeper increase well beyond the limit previously quoted.

A clear two peak structure at ± 1 in rapidity is observed, with a deep valley at $y = 0$. It should be noted that the heights of the forward and backward peaks are comparable if one chooses the gluon density parametrization according to Morfin-Tung set B1. However, the peak in the incident electron direction, positive rapidities in our convention, is much more pronounced if one uses a softer gluon density, like set B2 from Morfin-Tung. This observation conforms to our intuitive expectations.

It should be pointed out that the c-quark rapidity, as well as that of the D^*, is actually peaked at $y = 0$ if no cuts are applied. However, the cut in the momentum of the single pion in the decay $D^{*\pm} \to D^0\pi^\pm$ at 150 MeV gives rise to a depletion in the central rapidity region. This is due to the strong correlation between the energy of the single pion and the rapidity of the detected D^*.

Different relative behaviours can also be observed in the normalised $p_\perp$ distributions of the $D^{*\pm}$ reconstructed in the central tracking device. This is illustrated in Figure 4(b) where three different gluon parametrizations have been included.

We finally would like to point out that these features remain after cutting on the $p_\perp$ of the D^* at 1 or 2 GeV/c. Such a cut could be neccesary to get rid of competing processes.

5 Direct x_g reconstruction.

5.1 Methods of x_g calculation

In this section we recall some useful relations to calculate the momentum fraction carried by the gluon. They are based on the leading order process $\gamma g \to c\bar{c}$ shown in Figure 1. Considering the $c\bar{c}$-system as a whole three variables are needed to specify the kinematics.

The first quantity is the virtuality of the incoming photon, Q^2. In fact, because heavy flavour production cross-section peaks at so small values of Q^2 we will always use the collinear limit: $Q^2 \to 0$. To reinforce this approximation one can further require the non-observation of the scattered electron in the main detector.

As the second variable one usually takes the quantity y. In our limit, y equals the momentum fraction of the incoming electron carried by the photon and can be determined using the Jacquet-Blondel formula:

$$y = \sum_h \frac{E_i - P_{Li}}{2E_e} \tag{14}$$

where the sum runs over all particles measured in the calorimeter except for the scattered electron. In the interesting low-x_g region the use of the Jacquet-Blondel method seems to be problematic since some particles could escape through the beampipe hole in the rear direction. Figure 9(a) shows a nice correlation between the reconstructed y_{rec} and the generated value y_{exact}. The resolution is $\sigma_{JB} \sim 15\%$ (Figure 9(b)).

If we see the scattered electron in the main detector (which means that it should be scattered by more than 80 mrad) it is of course possible to calculate y, and also Q^2 –which cannot be neglected in this case–, using the relations:

$$y = 1 - \frac{E'_e}{2E_e}(1 - \cos\theta) \tag{15}$$

$$Q^2 = 2E_eE'_e(1 + \cos\theta)\,, \tag{16}$$

where θ is the polar angle of the scattered electron ($\theta = \pi$ meaning it has not been deflected).

If the electron is scattered by a very small angle, and it has lost enough energy to be bent out of the beampipe by the magnets to enter the electron tagger of the luminosity monitor, (15) simplifies to

$$y = 1 - \frac{E'_e}{E_e} \tag{17}$$

and we can safely neglect Q^2. This means that the electron should be scattered over less than 7 mrad, its energy should be between 13 and 24 GeV, and the maximum value of Q^2 that can be reached is 0.02 GeV^2. Because of the good energy resolution of the electron luminosity calorimeter, y can be measured with an accuracy of roughly 6% as shown in Figure 9(c). There are two problems with this event sample: only a small fraction of the electrons reach the luminosity system (less than about 10%) and the spanned y-range is limited to about 0.2 to 0.6. This would lead to distorted distributions if we only used these events.

So, to choose a specific method reduces to find an appropriate third variable allowing for the determination of x_g. We review some of them in the next section. Finally, we point out that alternative methods without the y-reconstruction requirement exist also. Their domain is, in some sense, complementary to the Jacquet-Blondel sensitivity region. They will also be presented in the next paragraphs.

5.1.1 Invariant mass reconstruction

We denote the momenta of the quarks by c and $\bar{c}$, to emphasize that we study heavy quark production, although most considerations also hold for light quarks. The gluon momentum is paramatrized to be $x_g P$, where P denotes the original proton energy. The photon momentum is denoted by q. The electron momentum is given by k. From momentum conservation we have

$$x_g P + q = c + \bar{c}\,. \tag{18}$$

Squaring gives

$$x_g^2 P^2 + 2x_g P\cdot q + q^2 = (c+\bar{c})^2\,. \tag{19}$$

Because we describe heavy quark production, we can safely neglect the first term and find for the momentum fraction of the proton carried by the gluon:

$$x_g = \frac{M_{c\bar{c}}^2 + Q^2}{2P\cdot q} = \frac{\hat{s}+Q^2}{ys}\,, \tag{20}$$

where $y \equiv P\cdot q/P\cdot P_e$ is the usual dimensionless Bjorken variable and $\hat{s} = M_{c\bar{c}}^2 = M_{\gamma g}^2$ is the squared partonic center-of-mass energy. In the collinear approximation ($Q^2 = 0$ and $q = y\,k$) the equation can be further simplified:

$$x_g = \frac{M_{c\bar{c}}^2}{ys} = \frac{M_{c\bar{c}}^2}{4E_\gamma E_e} = \frac{\hat{s}}{ys}\,. \tag{21}$$

To obtain $\hat{s}$ notice that this variable equals the square of the transverse mass of the produced quarks if the quarks are produced perpendicular to the beam in the γg-CM frame and if both the photon and the gluon had no initial transverse momentum ($Q^2 = 0$). So we can use the summed transverse mass of all final state particles as an approximation of this, which can be approximated by the summed transverse momenta:

$$\sqrt{\hat{s}} \approx \sum_i m_{\perp i} \approx \sum_i p_{\perp i} \tag{22}$$

It was shown in [43] that this is a good approximation when the produced quarks have a sizeable $p_\perp$.

Another possibility is to reconstruct the four-momentum of the hadron containing the heavy (anti)quark after the fragmentation process. Now, $\hat{s}$ can be calculated by using the following relation:

$$p_\perp^2 = z(1-z)\hat{s} - m_c^2 \tag{23}$$

with

$$z = \frac{P\cdot c}{P\cdot q} = \frac{(E-P_L)_c}{2yE_e} \tag{24}$$

A slight variation of this method was shown to work in the case of J/Ψ production [5].

5.1.2 Energy and longitudinal momentum conservation

A different approach is to look at the conservation of energy and longitudinal momentum separately. The positive z-axis is taken to be the direction of the incoming proton. We then have

$$\begin{aligned} x_g E_p + E_\gamma &= E_c + E_{\bar{c}}\,, \\ x_g P_p^L + P_\gamma^L &= P_c^L + P_{\bar{c}}^L\,. \end{aligned} \tag{25}$$

Adding gives

$$x_g = \frac{E_c + E_{\bar{c}} + P_c^L + P_{\bar{c}}^L - (E_\gamma + P_\gamma^L)}{2E_p}\,. \tag{26}$$

We have not done anything essentially different here than in the previous section, but the advantage turns up if we again go to the case where Q^2 can be neglected: since the photon moves in the negative z-direction, $E_\gamma = -P_\gamma^L$ now. so that x_g has no explicit dependence on y anymore:

$$x_g = \frac{E_c + E_{\bar{c}} + P_c^L + P_{\bar{c}}^L}{2E_p}\,. \tag{27}$$

Since energy and momentum is conserved in the fragmentation process too, this translates immediately into a sum over all final state particles coming from the $c\bar{c}$-system. The only condition is to remove the proton remnant debris from the final state and the scattered electron to get this system.

$$x_g = \frac{\sum_{c\bar{c}-syst}(E+P^L)}{2E_p}\,. \tag{28}$$

This looks like the Jacquet-Blondel equation (14) but essentially the role of the electron and proton are interchanged in the equation for x_g. At first sight, the only differences are the sign in the numerator and the appearance of the electron energy, instead of the proton energy, in the denominator. In the Jacquet-Blondel equation, the sum should run over all final-state particles (except for the scattered electron), but the negative sign in the numerator allows one to restrict the summation over all particles appearing in the detector, i.e. having a moderate rapidity. Thus, loss of particles in the forward beampipe does not harm the y-reconstruction using the Jacquet-Blondel formula. On the other hand, loss of particles in the rear beampipe gives serious trouble, especially if they are energetic.

In the case of equation (28), this is just the other way round: the sum should run over the final state, excluding the proton remnants, and loss of particles in the rear beampipe thus do not harm in our case. Due to the large Lorentz boost in the forward direction, and the strongly peaking cross-section there, the effect of including (loosing) a forward particle in the sum is much more drastic in our case than including (loosing) a backward one in the Jacquet-Blondel case. So separating the proton remnants from the rest of the hadronic system is essential.

5.1.3 Rapidity of the $c\bar{c}$ system

The determination of x_g and $\hat{s}$ can also be achieved by using the rapidity of the $c\bar{c}$-system [38,5]. In the photon-gluon center of mass frame the rapidities of the two quarks are opposite:

$$\hat{y}_c^0 = -\hat{y}_{\bar{c}}^0 \equiv D\hat{y}\,. \tag{29}$$

In the laboratory system this turns into:

$$\begin{aligned} \hat{y}_c &= \hat{y}_{\gamma g} + D\hat{y}\,, \\ \hat{y}_{\bar{c}} &= \hat{y}_{\gamma g} - D\hat{y}\,, \end{aligned} \tag{30}$$

so that:

$$\hat{y}_{\gamma g} = (\hat{y}_c + \hat{y}_{\bar{c}})/2 \equiv \bar{y}_{c\bar{c}}\,. \tag{31}$$

This gives

$$\hat{y}_{c\bar{c}} = \frac{1}{2}\ln\frac{E_p(x_g - \frac{Q^2}{s})}{yE_e}. \quad (32)$$

For photoproduction, where $Q^2 = 0$ this leads to expressions for x_g and $\hat{s}$, from only y and the rapidity of the two-jet system, $\hat{y}_{c\bar{c}}$:

$$x_g = \frac{yE_e}{E_p}\exp(2\hat{y}_{c\bar{c}}), \quad (33)$$

$$\hat{s} = 4E_e^2y^2\exp(2\hat{y}_{c\bar{c}}). \quad (34)$$

5.1.4 Jet rapidity and transverse jet mass

In $p\bar{p}$ (pp) physics, another method is widely used. For two jets in the final state, arising from a head-on collission of two partons, each carrying a momentum fraction x_i of the original particle, these x_i's can be expressed in rapidities of the two jets ($\hat{y}$ and $\hat{y}'$), and the transverse mass $m_\perp = m'_\perp = \sqrt{p_\perp^2 + m^2}$. In the center-of-mass system of the original colliding particles we have

$$x_{1,2} = \frac{m_\perp}{\sqrt{s}}\left[\exp(\pm\hat{y}^0) + \exp(\pm\hat{y}'^0)\right], \quad (35)$$

where s is the invariant mass of the $p\bar{p}$ (pp)-system. Translated to an asymmetric laboratory system, the equation reads:

$$x_{1,2} = \frac{m_\perp}{2E_{1,2}}\left[\exp(\pm\hat{y}) + \exp(\pm\hat{y}')\right], \quad (36)$$

In case of ep-scattering, we can calculate x_g and y from equation (36) in the collinear approximation ($Q^2 \sim 0$). If $E_1 = E_p$ and $E_2 = E_e$ then, $x_1 = x_g$ and $x_2 = y$. Note that we then also obtain $\hat{s}$ from

$$\hat{s} = x_1x_2s = 4m_{c\perp}^2\cosh\frac{\hat{y}_c - \hat{y}_{\bar{c}}}{2}. \quad (37)$$

5.2 Tagged D^* meson sample

In this section, we will discuss two methods of extracting the gluon structure function from an event sample in which reconstructed $D^{*\pm}$ mesons were used as a tag of the charm quark [39]. We will consider the production of $c\bar{c}$ via the BGF mechanism[6].

One advantage of reconstructing exclusive channels is that there is no need for jet reconstruction, the disadvantage being the low tagging efficiency. Two questions arise here:

- How well can we reconstruct D^*'s?
- How accurately does the D^* momentum represent the momentum of the charm quark?

The answer to the first question comes partly from section 3.1. It was shown that it is possible to get a relatively clean D^* sample. Furthermore Figure 7 shows a nice correlation between generated and reconstructed kinematical parameters of the $D^{*\pm}$ mesons. The

[6]Resolved photon events can also be used to extract x_g. This requires a correct treatment of the photon remnants. See [5] for the J/Ψ case. The possibility of measuring the hadronic structure of the photon using a tagged photon beam at HERA is discussed in [40].

chosen quantities are $cos\theta$ (Figure 7(a)), and its momentum P (Figure 7(b)). Approximate descriptions of the following effects were included in the distributions: detector resolution and acceptance, trigger and reconstruction.

The answer to the second question can be obtained by comparing quantities related to the generated D^* meson and the corresponding quantities of the parent charmed quark. Figure 8 shows there is a quite good correlation between the generated and the reconstructed numbers for $cos\theta$ (Figure 8(a)) and P (Figure 8(b)) distributions. A correction has to be applied due to fragmentation effects, namely, the D^* meson only carries a certain fraction of the c quark momentum (of the order of 70% as measured in e^+e^- experiments [41]). There are two ways of correcting for this effect:

- either by taking into account all particles within a cone of a certain angle (20 to 30°) around the D^* direction : $\vec{D}^*_{corr} = \vec{D}^* + \vec{P}_{cone}$
- or by using the fragmentation function : $\vec{D}^*_{corr} = \vec{D}^*/ < x_D >$.

A first method to derive x_g is to use the expression (23). Inclusive D^* events were used as a tag of one charm quark. Figure 10(a) shows the correlation between the exact value x_g^{gen} and the reconstructed x_g^{rec} after a correction using the second method with $< x_D >= 0.7$. A minimum $p_\perp(D^*)$ of 1.4 GeV/c was required. The distributions correspond to 6 pb^{-1}. Denoting the relative error by $\frac{\Delta x_g}{x_g}$, the mean value $< \frac{\Delta x_g}{x_g} >$ is $\sim 0.7\%$ and the resolution is $\sim 40\%$ (Figure 10(b)). We see that x_g can be determined in the range $5 \times 10^{-4} \leq x_g \leq 10^{-1}$. Similar results, with somewhat better resolution, were obtained for hidden charm (J/Ψ) production [42,16].

A second method of extracting x_g consists of determining the rapidity $\hat{y}_{c\bar{c}}$ of the partonic system (equation (32)). One can either simulate the charmed quarks by using reconstructed $D^{*\pm}$ ($\hat{y}_{c\bar{c}} \sim \hat{y}_{D^{*+}D^{*-}}$) or tag one charmed quark and reconstruct the hardest hadron in the opposite direction ($\hat{y}_{c\bar{c}} \sim \hat{y}_{D^*hadron}$).

Figure 11(c) shows a nice correlation between the reconstructed $\hat{y}_{D^{*+}D^{*-}}$ and the exact value $\hat{y}_{c\bar{c}}$. The corresponding x_g correlation plot is shown in Figure 11(d). The mean value $< \frac{\Delta x_g}{x_g} >$ is $\sim 16\%$. A resolution $\sigma(\frac{\Delta x_g}{x_g}) \sim 28\%$ can be achieved (Figure 11(a)); $\frac{\Delta x_g}{x_g}$ is rather constant over the whole x_g range $10^{-3} \leq x_g \leq 3 \times 10^{-2}$ (Figure 11(b)). With a cross-section of ~ 10 pb, this method results in a smaller sample than that discussed above. However, events with one reconstructed D^* and one reconstructed jet axis or a hadron in the opposite direction can be used to increase the statistics. By requiring a hadron momentum of at least 1.5 GeV/c and the angle between the D^* and the additional hadron satisfying $cos\theta_{D^*-h} \leq -0.9$, the cross-section is of the order of 100 pb. Using this method, x_g can be determined in the range $6 \times 10^{-4} \leq x_g \leq 10^{-1}$ with a mean value $< \frac{\Delta x_g}{x_g} > \sim 4\%$ and a resolution $\sigma(\frac{\Delta x_g}{x_g}) \sim 37\%$.

5.3 Full hadronic final states and jets

If we can identify the heavy quark events with hadronic final states by using, e.g., the $D^{*\pm}$ tagging method described in section 3.1 (a good tag is needed due to the huge light-quark background), we can also use the whole hadronic final state for the x_g-determination. We can try to reconstruct both quark jets by using a suitable jet algorithm. The main problem is that it is not possible to determine unambiguously which final state particles originate from

which partons: their hadronization products are not perfectly separated into two narrow jets. We have used two types of cluster algorithms:

- LUCLUS type 1, which uses the relative transverse momentum as a clustering parameter (distance measure between two particles/ jets):

$$R_T^2 \equiv 2\frac{|\vec{p}_1|^2|\vec{p}_2|^2}{(|\vec{p}_1|+|\vec{p}_2|)^2}(1-\cos(1,2)). \tag{38}$$

- Another distance measure is

$$D_{1,2} \equiv 1 - 2\sqrt{2}\,\frac{|\vec{p}_1||\vec{p}_2|\sqrt{(1-\cos(1,2))}}{(|\vec{p}_1|+|\vec{p}_2|)^2} = D_{2,1} \tag{39}$$

This measure is dimensionless, $0 \leq d_{12} \leq 1$ and

$$D_{i,j} = \begin{cases} 1 & \text{for identical objects} \\ 0 & \text{for extremely different objects} \end{cases} \tag{40}$$

Because of this, D is also called 'similarity'.

Clustering proceeds by combining particles which are most similar and the algorithm is stopped when the clustering parameter reaches a predefined cut-off value or when a predefined number of jets is reached. After this, some quality cuts are applied on the jet candidates, rejecting or accepting the event accordingly. The performance of the first method depends on the optimized distance definition and the kind of process involved, giving the right multiplicity in most cases without further cuts. However, the efficiency is low. In the second method, the output is independent of the multiplicity of the input jets, thus, it will give the desired topology irrespective of the input number of jets, yielding a high efficiency. Quality cuts must be devised in order to assure an acceptable purity of the sample.

Charm events were generated with AROMA[46], followed by a fast detector simulation with track smearing and beam pipe cuts. The gaussian smearing in momentum and angular variables for charged particles was done according to the design values from reference [47]. Neutral particles were smeared according to $\sigma_E = 18\%\sqrt{E}$, $\sigma_\theta = \sigma_\phi = 3\ mrad$. Only events with $\sum E_\perp \geq 5\ GeV$ were accepted in the analysis in order to roughly simulate first level trigger cuts.

The clustering was done as described above and stopped when the number of jets was three. Two of these jets were identified as current jets and the third one, as a beam pipe jet. This identification was done according to the angle between the jets in the transverse plane, where the c and $\bar{c}$ jets must be approximately back-to-back. Hence, the pair with transverse opening angle bigger than 150°, was chosen as the current jet pair. The third jet was considered to be the spectator jet and consequently discarded.

The efficiency of this method, after the cut on the transverse opening angle is above 90%. Figure 12 shows the jet energy ($\Delta E/E$) and angular ($\Delta\theta/\theta$ and $\Delta\phi/\phi$) resolutions for $c\bar{c}$ events after reconstruction and acceptance. As can be seen from this figure, a fairly good reconstruction is achieved. Distributions are centered at zero, though they present tails and asymmetries which are due to particle losses into the beam pipe.

After the jets are reconstructed, x_g can be determined via equation (21). Figure 12 also shows $\Delta x_g/x_g$ as a function of x_g in the sensitivity range 10^{-3} to 10^{-1} .

Usually most of the proton remnants are lost in the beampipe, but not all of it. When the jet finding algorithm is applied, it may happen that the remnant particles are assigned to one of the BGF jets, or even give rise to another jet outside the beampipe. To control this, we can insert a fake particle in the beampipe which simulates the lost particles. This will then form a jet in the beampipe, and the remnant particles which were seen in the detector will be assigned to this jet too. We can then remove this jet from the final hadronic system, and are left with the particles arising from the produced quarks. The square of their summed momenta gives $\hat{s}$. This method has the advantages that we do not have to specify which particle belongs to which jet (quark) and that we do not have to restrict ourselves to the two-jet events only.

In Figure 13 the results are shown for x_g reconstruction using jets in $b\bar{b}$-events, without and with this trick. These plots are made for 1000 bottom events generated with GAMGLU[45] without any kinematical cuts. The structure functions EHLQ set 1 are used, and the mass of the b is set to $m_b = 5.0\ GeV$. After smearing, a beampipe cut ($0.1 rad$) and removal of the scattered electron, LUCLUS is applied with $R_T^{max} = 3\ GeV$ with and without this fake particle inserted. About 60 % of all generated events give rise to 2-jets. These are used as the final event sample.

We show the results using the energy and P_L of the two clusters (equation(28)). If we do not include the proton remnants, the distribution $\Delta x_g/x_g$ gets a tail on the high side and has a spread ~ 0.3 (Figure 13(a,b)). The scatter plot shows where this tail comes from: we have an extra band just above the diagonal. With the trick mentioned before, the distribution is more or less symmetrical and has a $r.m.s. \sim 0.2$ (Figure 13(c,d)). The extra band in the scatter plot has also disappeared. The distribution has a small shift, which is caused by the loss of a part of the particles from the $b\bar{b}$-system.

The major unsolved problem for $b\bar{b}$ events is to extract a clean sample. A possibility is to consider quantities like circularity and $p_\perp(jet)$ as input for a neural network. However, none of these quantities is powerful enough by itself.

5.4 $c\bar{c} \to l^+l^-X$ events

Once that a hard l^+l^- pair has been tagged, one is confident of having triggered an event with two heavy quarks entering the detector region. A measure of x_g is possible if one is able to reconstruct the rapidity of the $c\bar{c}$ -system and the energy of the incoming photon. As already seen, the definition of the variable δ equals, for not very large values, the Jacquet-Blondel method of y-reconstruction or, even better, the product $\delta.E_e$ simulates the incoming-γ momentum, in spite of more or less collinear electromagnetic initial state radiation. In Figure 14 the correlation between δ^{rec} and y^{gen} is shown. Notice that the region of *delta*-variation is bounded by our triggering cut, $\delta \leq 0.55$. Figure 14 shows that there is a bias in the Bjorken-y reconstruction, the values of δ being systematically lower. This is a usual feature of the Jacquet-Blondel method due to the particle losses into the beam pipe. In our particular case, there is another more important source of mismatching, namely, the existence of two energetic neutrinos accompaning the lepton pair.

The reconstruction of $\hat{y}(c\bar{c})$ can well be approximated by the rapidity of the lepton pair [5]. This is documented in Figure 15 where we plot $\hat{y}(e^+e^-)$ versus $\hat{y}(c\bar{c})$. As we can see, the correlation is not very much distorted afer inclusion of the remaining background contribution.

We have calculated x_g by using the following relation:

$$x_g^{rec} = \frac{\delta^{rec} E_e}{E_p} \exp\left(2\ \hat{y}(e^+c^-)\right) \tag{41}$$

The quality of the reconstruction is illustrated in Figure 16. We are sensitive to values $3 \times 10^{-4} \leq x_g \leq 3 \times 10^{-1}$ with a bias $< \frac{\Delta x_g}{x_g} > \sim 4\%$ and a resolution $\sim$ 60%.

Now we have all the information for further calculation of $\hat{s}$, that is used as the mass scale for the gluon density function. Notice that the mean value of $\hat{s}$ is a strongly changing function of x_g:

$$< \hat{s} > (x_g) \sim 10^4\ x_g\ GeV^2 \tag{42}$$

The correlation between the generated versus the reconstructed numbers has been plotted in Figure 17. The order of magnitude is reproduced but this is enough since the Altarelli-Parisi evolution equations predict a logarithmic scale dependence.

6 Unfolding of the gluon density

Having reconstructed x_g we now proceed to determine the gluon function. It is related to the measured cross-section via:

$$G(x_g, \mu^2(x_g)) = \frac{d\sigma/dx_g|_{exp}}{f(x_g)|_{MC}} \tag{43}$$

where

$$f(x_g)|_{MC} = d\sigma/dx_g|_{MC}/G(x_g)|_{MC} \tag{44}$$

was determined by the Monte Carlo program, including full detector simulation.

The bin sizes were chosen by requiring statistical errors smaller than 5% for an integrated luminosity of 100 pb^{-1}. We further demand that migrations between bins satisfy the Longo criteria: After taking the experimental resolutions into account, more than 60% of the original events of a bin remain inside this bin. Moreover, the fraction of events which migrate into this bin is smaller than 40%. These conditions lead, in particular, to approximate regular bin sizes in the variable $log(x_g)$.

Even with perfect measurements a finite bin width introduces a systematic shift if $d\sigma/dx_g$ varies inside a bin. This effect can be reduced by reconstructing the gluon density for each bin at the point $(< log(x_i^{rec}) >, < log(\hat{s}_i^{rec}) >)$.

After all conditions are satisfied one can be confident that the relation (43) gives a reliable approximation to $G(x_g)$. The net systematic error can be then computed by varying the Monte Carlo functions $f|_{MC}$ using different gluon parametrizations [48,5].

Figure 18 shows that one can discriminate among different parametrizations of the gluon density $G(x_g)$ (in this case the input densities used are from Morfin and Tung Sets B1 and B2 [36]). The figure does not include systematic errors and the statistical errors correspond to 6 pb^{-1}. In Figure 19 we show the measured gluon density as obtained from set B2 of Morfin and Tung. For comparison, we have also included two input functions evaluated at $\mu^2 =< \hat{s} > (x_g)$ as given by relation (42). To give an idea of the uncertainties entering the theoretical definition of $G(x_g, \mu^2)$ we assume a relative factor of two in the squared value of the mass scale. We see that we are able to discriminate between current parametrizations having different behaviours at very low x_g.

7 Summary and Conclusions

In this work we have investigated the prospects of extracting the leading order gluon density from open charm production in ep collisions at HERA energies. The results have been obtained by using fully detector-simulated signal and background events. The reconstruction of event kinematics has been carefully outlined, in particular uncertainties due to higher order corrections have been discussed. Initial and final gluon radiation was implemented using a parton shower approach. Background events were mainly produced via the resolved component of the photon.

Tagging of the events was performed by using two standard methods, namely, $D^{*\pm}$ reconstruction using the process $D^{*\pm} \rightarrow D^0\pi^\pm \rightarrow (K^\mp\pi^\pm)\pi^\pm$, and leptonic decays of both charmed hadrons ($c\bar{c} \rightarrow l^+l^-\ X$). With a charm cross-section of $O(600\ nb)$ and an integrated luminosity of 100 pb^{-1}, $O(10^5)$ $D^{*\pm}$ and $O(10^4)$ l^+l^- events can be reconstructed per year. These tagged charm events were used to extract the momentum fraction of the proton carried by the gluon, x_g, in the range $10^{-3} \leq x_g \leq 10^{-1}$. An adequate discrimination among different parametrizations can be achieved even with moderate luminosities.

We conclude that charm production at HERA is well suited for a measurement of the gluon density for the following reasons:

- Comfortable production rates.
- Direct sensitivity to the gluon density.
- Well defined tagging algorithms.
- Wide range in x_g, allowing to distinguish between alternative parametrizations.

However, further studies are required to understand the effects of radiative corrections, backgrounds and systematic error computation in general. Real experimental data will help to clarify also these points.

Acknowledgements

We thank A. Ali, G.A. Schuler, M. Drees and D. Monaldi for useful discussions. Two of us (F.B. and J.F. de T.) would like to thank the Alexander von Humboldt Stiftung and the Kfz. Karlsruhe, respectively, for supporting their stays at the University of Bonn and at DESY during the summer of '91 when part of this work was performed. We acknowledge A. Ali and G. Wolf for a critical reading of the manuscript.

References

[1] A. Ali et al., in Proc. of HERA Workshop, DESY, Hamburg, FRG, Vol.1 (1988) 393; R.D. Peccei (Ed.).

[2] A.C. Benvenuti et al. (BCDMS Coll.), Phys. Lett. **B233** (1989) 490.

[3] P. Berge et al. (CDHSW Coll.), Z. Phys. **C49** (1991) 187.

[4] J.C. Collins, D.E. Soper and G. Sterman, Nucl. Phys. **B263** (1986) 37.

[5] K.J. Abraham, H. Jung, G.A. Schuler and J. F. de Trocóniz in Proceedings of the EFCA Workshop on LHC Physics, Aachen, FRG (1990).

[6] G.A. Schuler, Nucl. Phys. **B299** (1988) 21.

[7] E. Eichten, C. Quigg, I. Hinchliffe and K. Lane, Rev. Mod. Phys. **56** (1984) 579.

[8] G. Ingelman and G.A. Schuler, Z. Phys. **C40** (1988) 299.

[9] R.K. Ellis and Z. Kunszt, Nucl. Phys. **B303** (1988) 653.

[10] M. Drees and R.M. Godbole, Phys. Rev. **D39** (1989) 169.

[11] P. Nason, S. Dawson and R.K. Ellis, Nucl. Phys. **B303** (1988) 607.

[12] R.K. Ellis and P. Nason, Nucl. Phys. **B312** (1989) 551.

[13] J. Smith and W.L. van Neerven, New York Univ. at Stony Brook, preprint ITP-SB-91-40.

[14] R.K. Ellis and D.A. Ross, Nucl. Phys. **B345** (1990) 79; J.C. Collins and R.K. Ellis Nucl. Phys. **B360** (1991) 3.

[15] S. Catani, M. Ciafaloni and F. Hautmann, Phys. Lett. **B242** (1990) 97.

[16] F. Ould-Saada, in Proc. 4^{th} Symp. on Heavy Quark Physics, Orsay 25-29 June 1991 and DESY 91-138.

[17] J.C. Anjos et al. (Tagged Photon Spectrometer Coll.), Phys. Rev. Lett. **62** (1989) 513.

[18] J.C. Anjos et al. (Tagged Photon Spectrometer Coll.), Phys. Rev. Lett. **65** (1990) 2503.

[19] J.J. Aubert et al. (European Muon Coll.), Z. Phys. **C35** (1987) 1.

[20] Heavy Flavors and High Energy Collisions in the 1-100 TeV Range, Ettore Majorana Int. Science Series, Vol. 44 (1989), A. Ali and L. Cifarelli (Eds.) (Plenum Press, N.Y., 1989).

[21] L.V. Gribov, E.M. Levin and M.G. Ryskin, Phys. Rep. **100** (1983) 1.

[22] V.N. Gribov and L.N. Lipatov, Sov. J. Nucl. Phys. **15** (1972) 78.

[23] G. Altarelli and G. Parisi, Nucl. Phys. **B126** (1977) 298.

[24] M. Bengtsson, G. Ingelman and T. Sjöstrand, in Proc. of HERA Workshop, DESY, Hamburg, FRG, Vol.1 (1988) 149; R.D. Peccei (Ed.).

[25] H.-U. Bengtsson and T. Sjöstrand, to be published.

[26] D. Monaldi, private communication.

[27] F. Ould-Saada, H1-Note-05/91-173.

[28] F. Barreiro, J. del Peso and J.F. de Trocóniz, ZEUS-Note-91-122.

[29] Y. Eisenberg, C. Glasman, U. Karshon and A. Montag, to be published.

[30] G.J. Feldman et al., Phys. Rev. Lett. **38** (1977) 1313.

[31] M. Procario (CLEO Collaboration), in Proc. 11^{th} Intenational Conference on Physics in Collision, Colmar, France 20-22 June 1991.

[32] J. Buerger et al., H1-03/91-164, PRC-91-01.

[33] S. Egli, in Proc. 3^{rd} Topical Seminar on Heavy Flavours, San Miniato 17-21 June 1991.

[34] J. del Peso and J.F. de Trocóniz, ZEUS-Note 91-060 and references therein.

[35] H. Albrecht et al. (ARGUS Collaboration). DESY 91-112.

[36] J.G. Morfín and W.K. Tung, Z. Phys. **C52** (1991) 13.

[37] D. Feeken, Diplomarbeit, Hamburg 1991.

[38] The method is used quite often. It is documented in several books, e.g., W. Hoffmann, Jets of Hadrons (Springer, 1981), and the kinematics at the basis can be understood with E.Byckling, K.Kajantie, Particle Kinematics (John Wiley & Sons, 1973).

[39] F. Ould-Saada, H1-Note-05/91-199.

[40] R.S. Fletscher, F. Halzen, S. Keller, W.H. Smith, MAD/PH/633, BA-91-17 (March 1991).

[41] W. Braunschweig et al. (TASSO Coll.), Z. Phys. **C44** (1989) 365.

[42] H. Jung et al., these proceedings.

[43] G. d'Agostini and D. Monaldi, Z. Phys. **C48** (1990) 467.

[44] T. Sjöstrand, JETSET 7.2, CERN November 1989.

[45] J.J. Engelen, S.J. de Jong, M. Poletiek, J.A.M. Vermaseren, GAMGLU2.0, Z. Phys. **C41** (1988) 173.

[46] G. Ingelman and G. Schuler, DESY preprint in preparation.

[47] ZEUS Collaboration, ZEUS detector status report, DESY 1991.

[48] A.M. Cooper-Sarkar et al., in Proc. of HERA Workshop, DESY, Hamburg, FRG, Vol.1 (1988) 231; R.D. Peccei (Ed.).

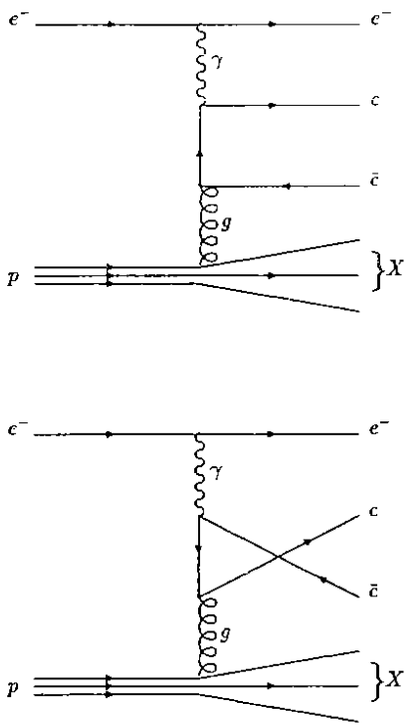

Figure 1

Lowest order boson-gluon fusion diagrams for charm production processes $ep \to ec\bar{c}X$.

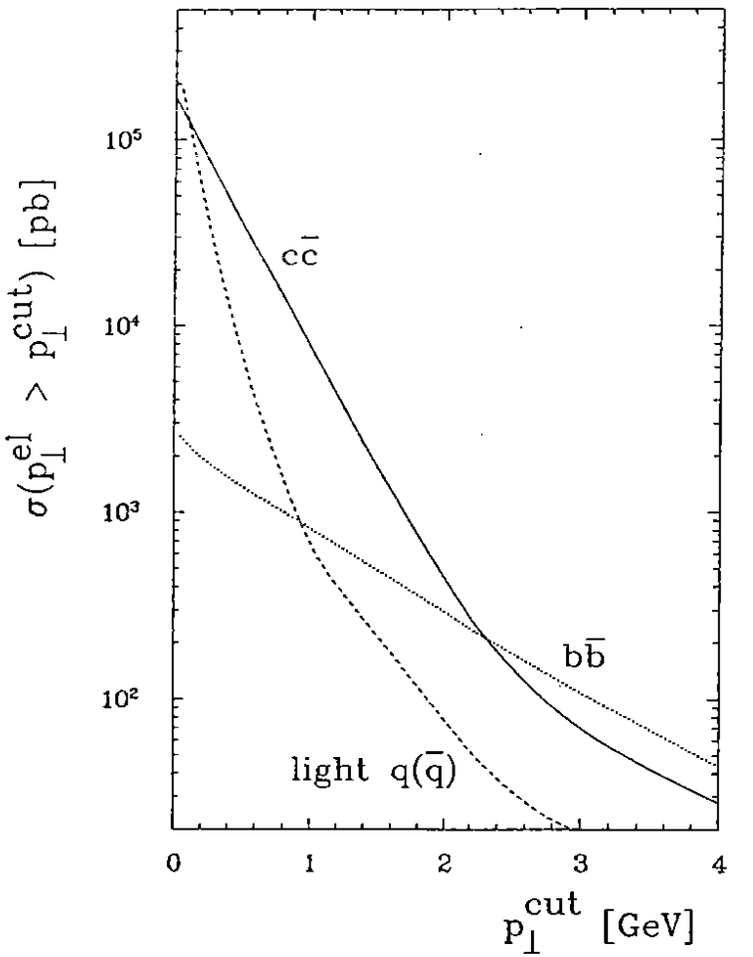

Figure 2

Inclusive cross section as a function of the electron $p_\perp$-cut for $c\bar{c}$, $b\bar{b}$ and light quark events.

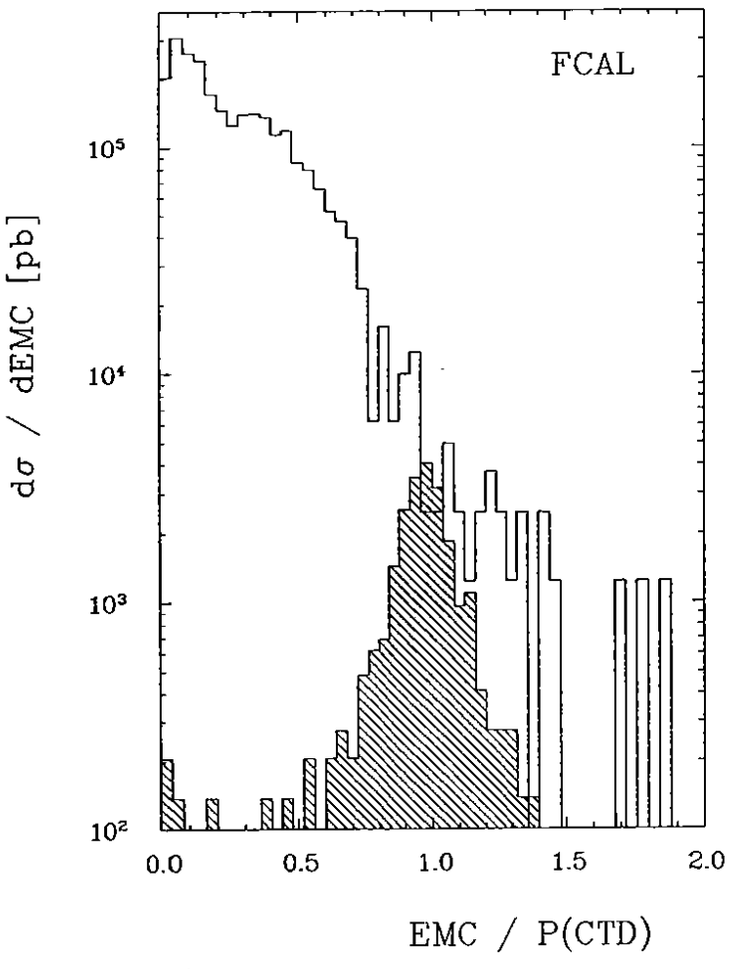

Figure 3

Inclusive charged track cross-section as a function of EMC/P where EMC is the electromagnetic energy measured in the calorimeter (FCAL) and P is the momentum given by the central tracking device (CTD). The shaded histogram corresponds to electrons and the open one to hadrons.

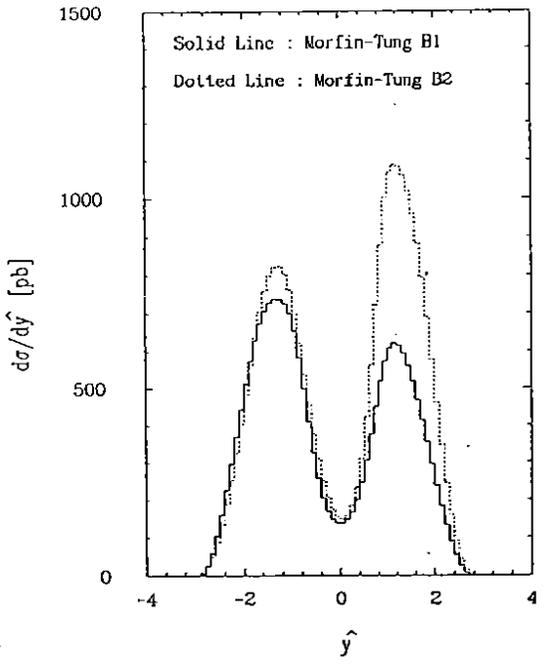

(a)

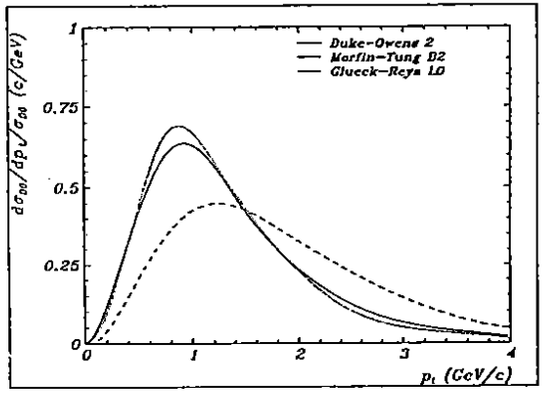

(b)

Figure 4

(a) Rapidity distributions for reconstructed $D^{*\pm}$ corresponding to sets B1 (solid histogram) and B2 (dashed histogram) of Morfin and Tung [37]. (b) Normalized distributions of transverse momentum of $D^{*\pm}$ within the central traking region.

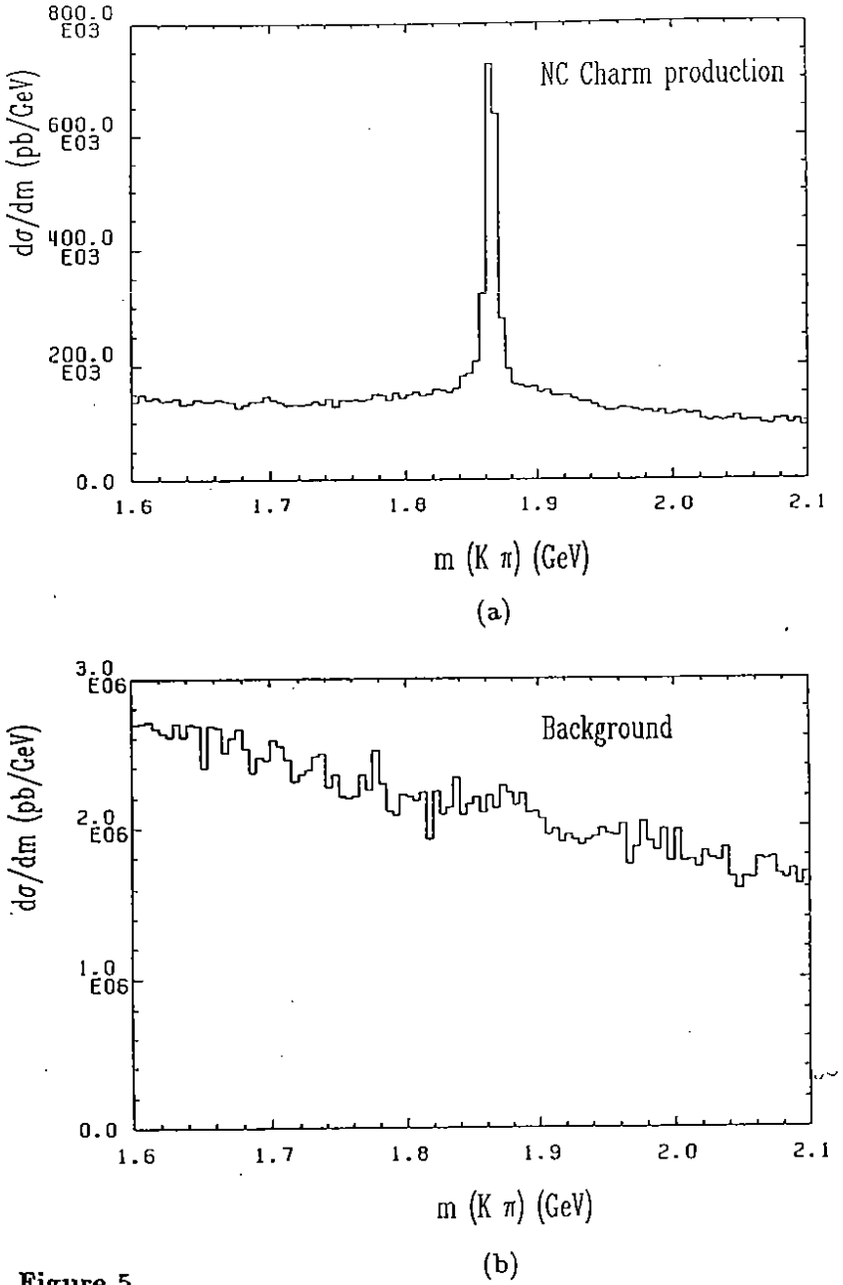

Figure 5

Invariant Mass Distribution $M(K^-\pi^+)$ for $c\bar{c}$ (a) and background events (b).

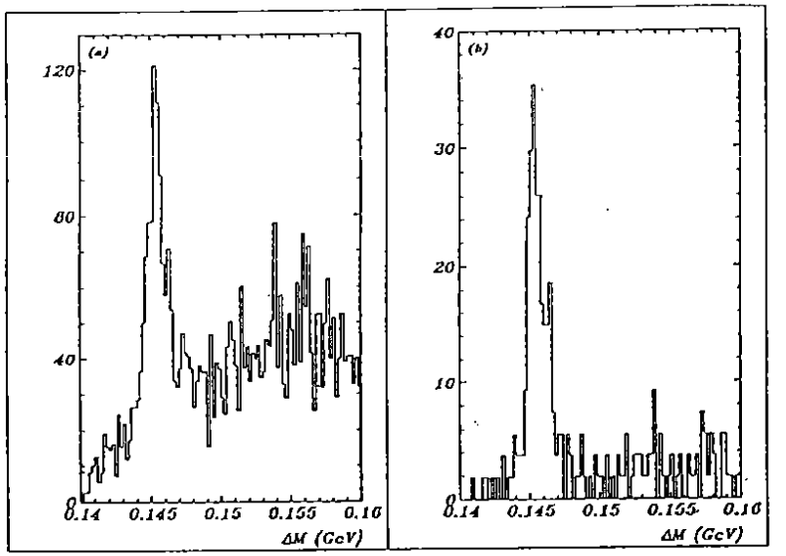

Figure 6

$\Delta M = M(K^-\pi^+\pi^+) - M(K^-\pi^+)$ mass difference for $c\bar{c}$ and background events before (a) and after (b) vertex constraint.

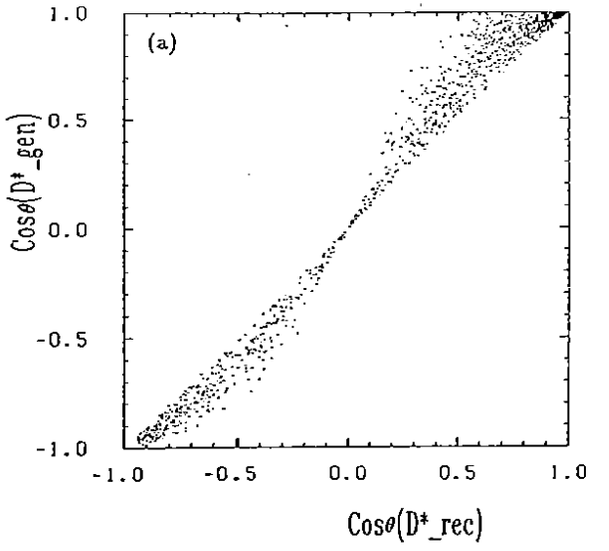

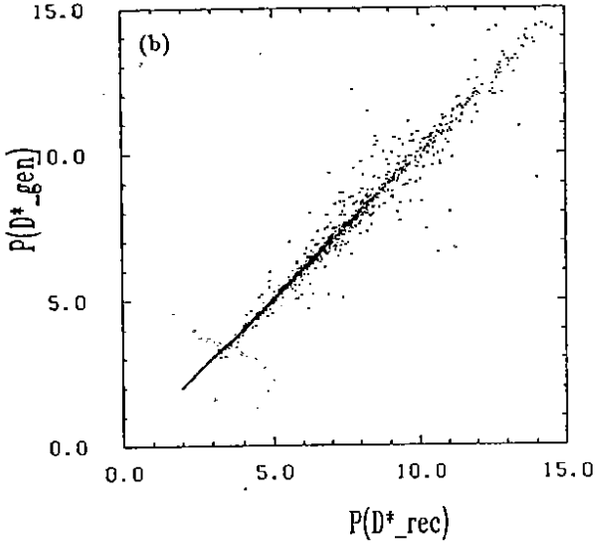

Figure 7

Correlation between reconstructed $D^{*\pm}$ quantities and generated ones: (a) $cos\theta$ and (b) absolute momentum P.

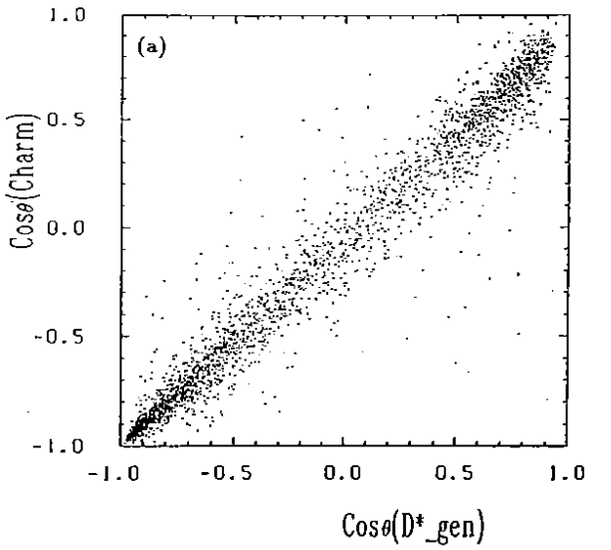

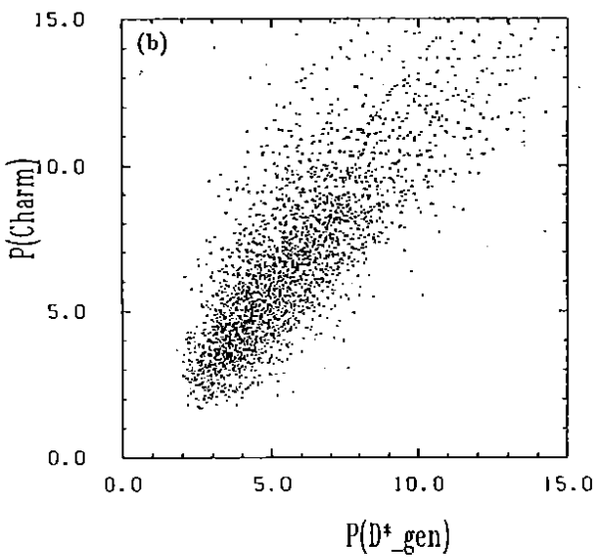

Figure 8

Correlation between generated $D^{*\pm}$ quantities and parent charm quantities: (a) $cos\theta$ and (b) momentum P.

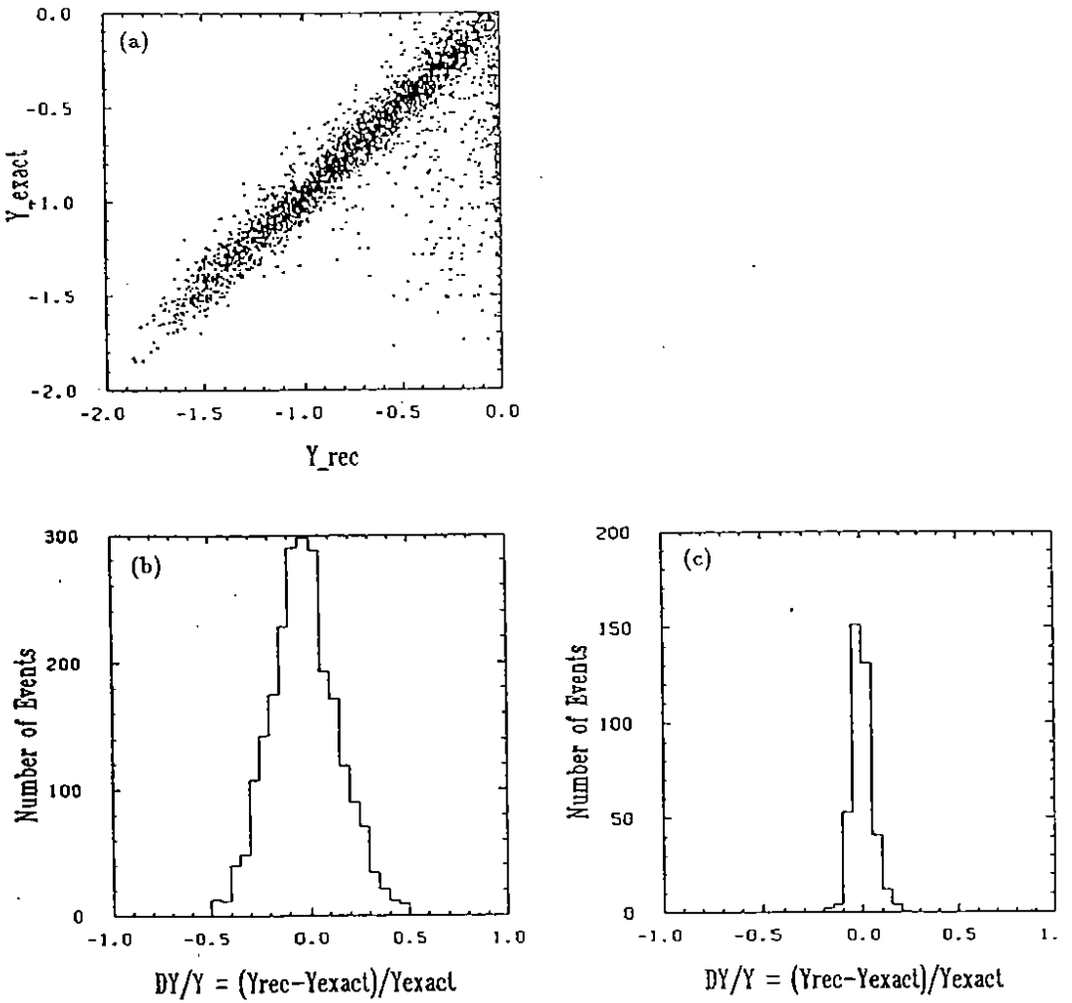

Figure 9

Correlation y_{rec} versus y_{exact} for $c\bar{c}$ production (a) and relative error $\Delta y/y$ (b) where y_{rec} was determined using the Jacquet-Blondel method. Also shown is the relative error $\Delta y/y$ when using the electron tag method (c).

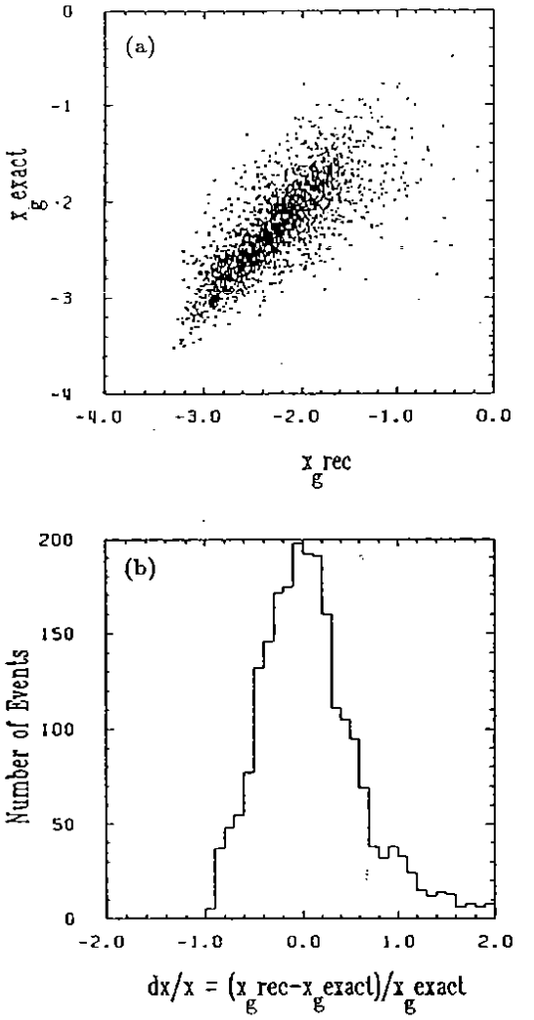

Figure 10

x_g determination using inclusive reconstructed $D^{*\pm}$ mesons as a tag of the charmed quark: correlation x_g^{rec} versus x_g^{exact} (a) and relative error $\Delta x_g/x_g$ (b).

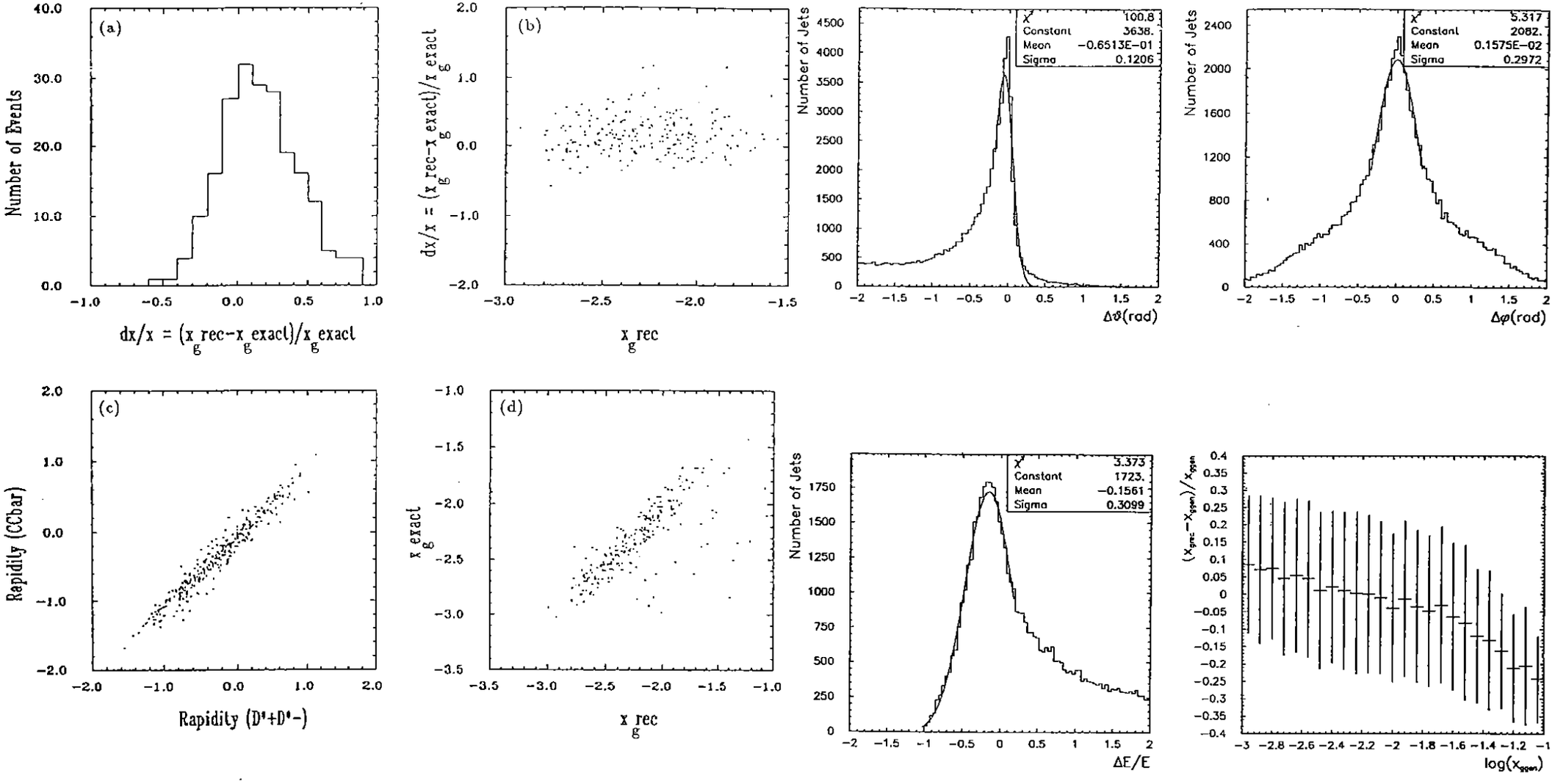

Figure 11

x_g determination using reconstructed $D^{*+}D^{*-}$ events as a tag of $c\bar{c}$: relative error $\Delta x_g/x_g$ (a), $\Delta x_g/x_g$ versus x_g (b), $\hat{y}_{c\bar{c}}$ versus $\hat{y}_{D^{*+}D^{*-}}$ (c) and x_g^{exact} versus x_g^{rec} (d).

Figure 12

Jet energy and angular resolutions for $c\bar{c}$ events together with the relative error $\Delta x_g/x_g$ versus x_g .

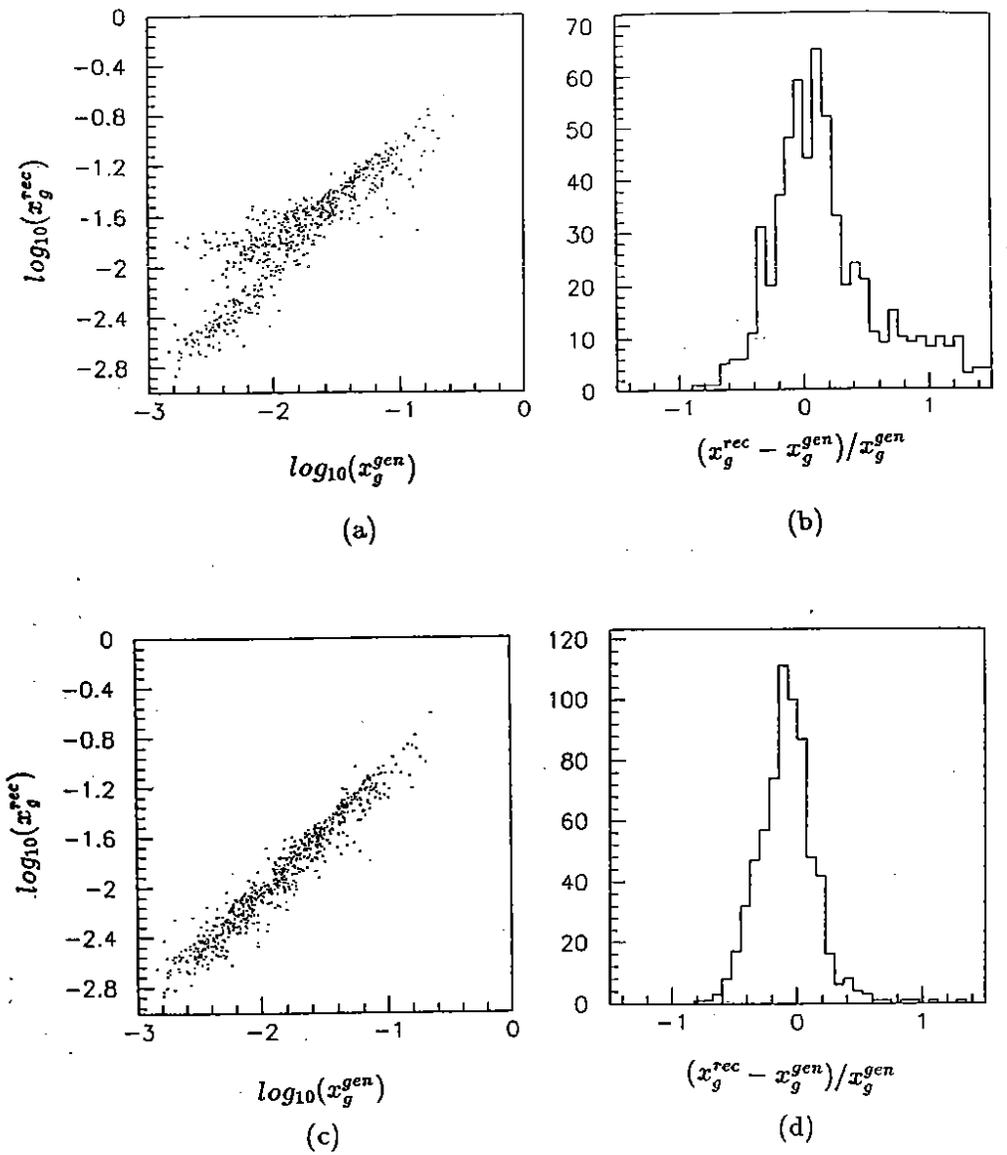

Figure 13

x_g determination using hadronic final states and jets: correlation $x_g^{E+P_l}$ (equation (28)) versus x_g^{exact} (a) and relative error $\Delta x_g/x_g$ (b) and the same plots with the fake proton remnant inserted in the beampipe (c) and (d).

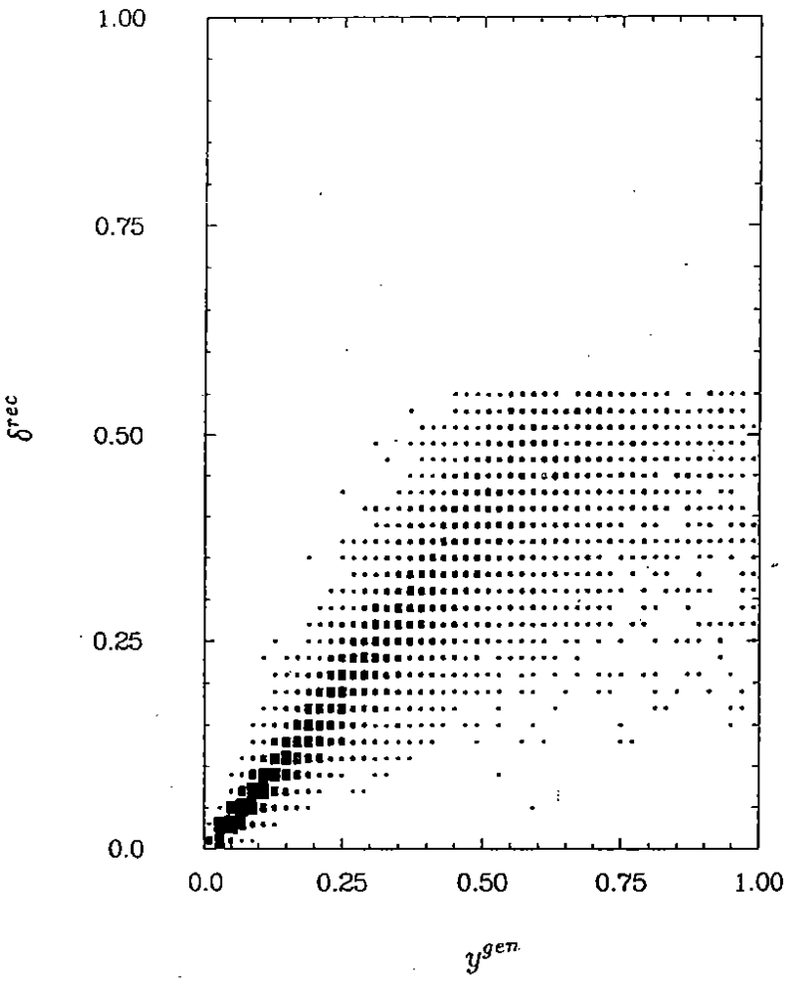

Figure 14

Correlation between Bjorken-y and δ (as defined in the text) for dileptonic tagged charm and background events after full detector simulation. The triggering cut, $\delta \leq 0.55$ is explicitely shown.

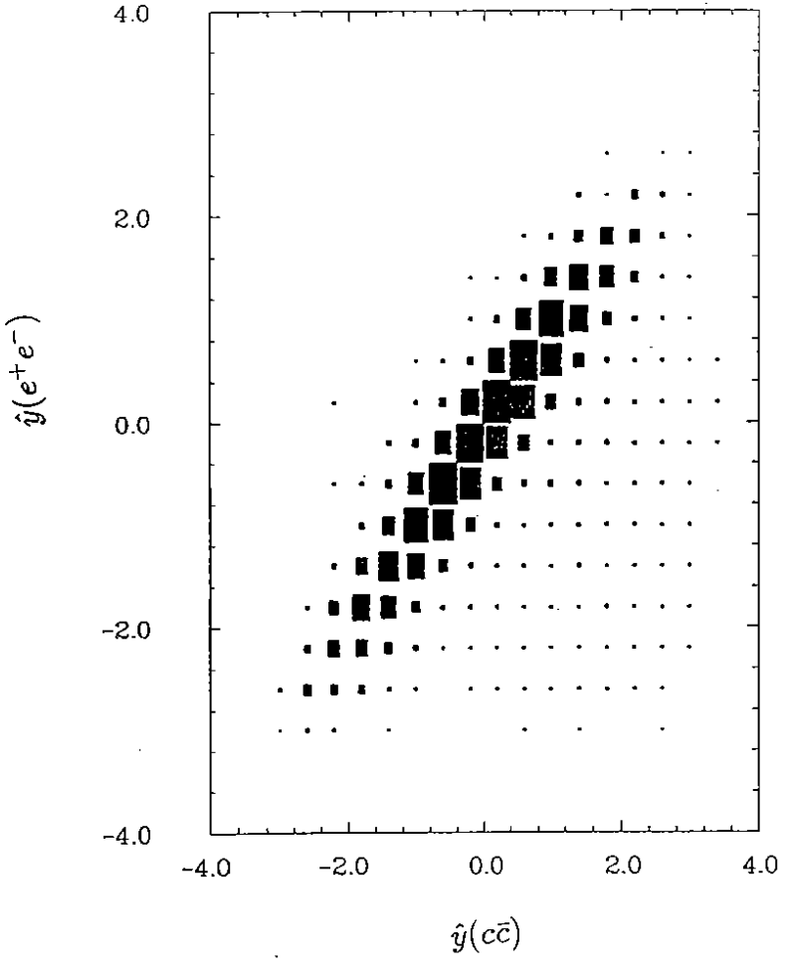

Figure 15

Correlation between $\hat{y}(c\bar{c})$ and $\hat{y}(e^+e^-)$ as measured in the laboratory frame for dileptonic tagged charm and background events after full detector simulation.

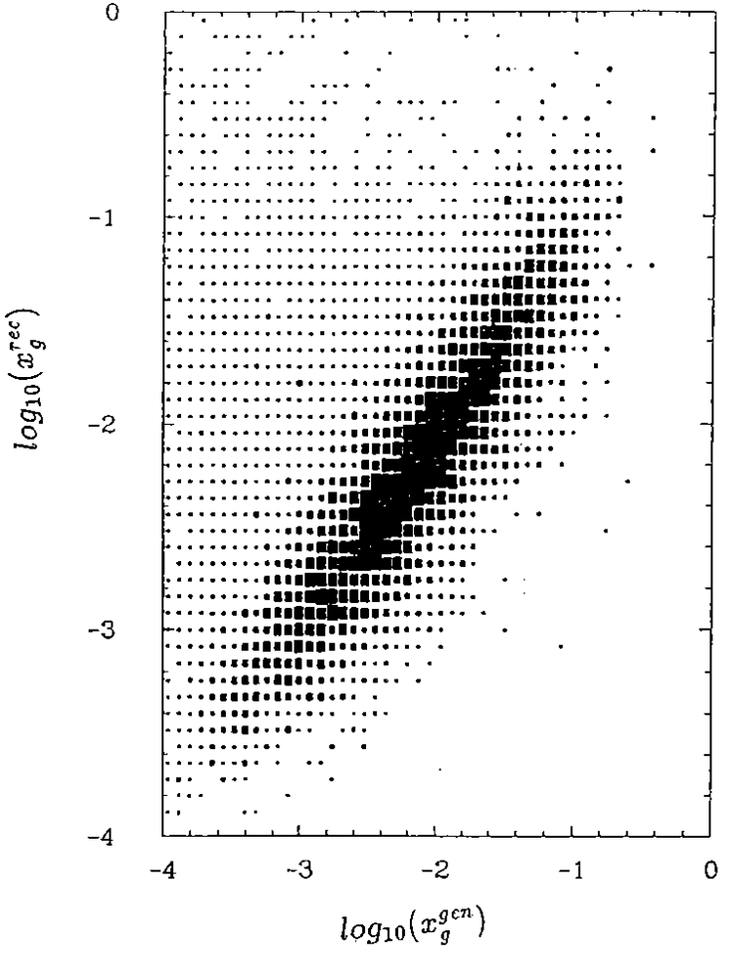

Figure 16

Correlation between the generated and reconstructed x_g for dileptonic tagged charm and background events after full detector simulation.

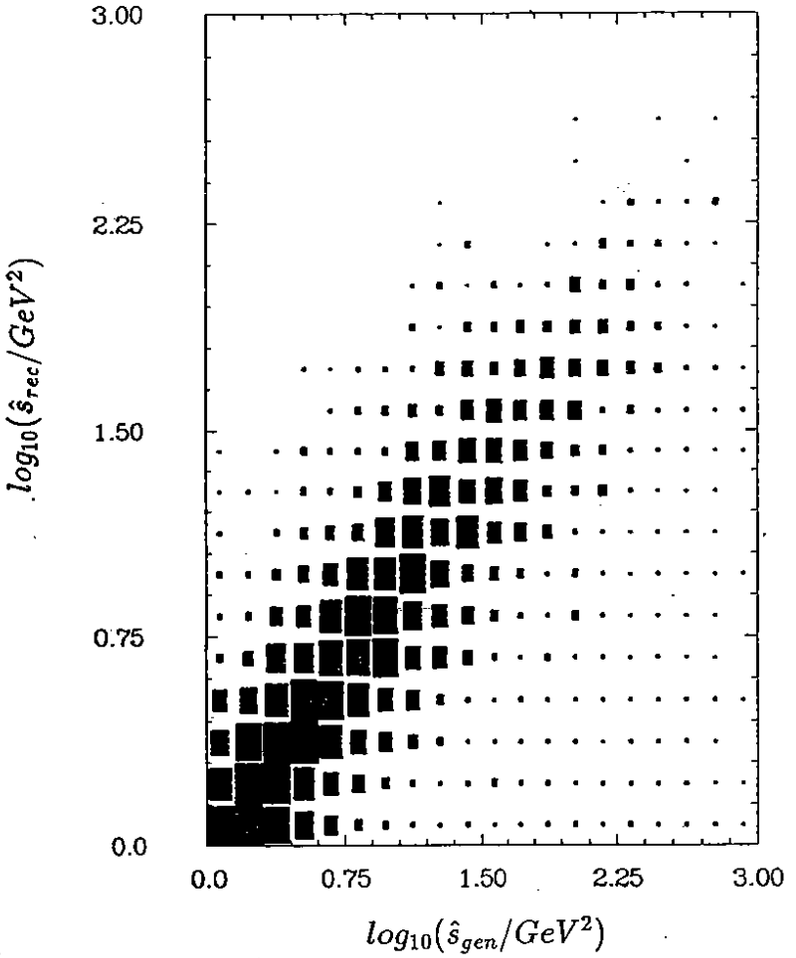

Figure 17

Correlation between the generated and reconstructed $\hat{s}$ for dileptonic tagged charm and background events after full detector simulation.

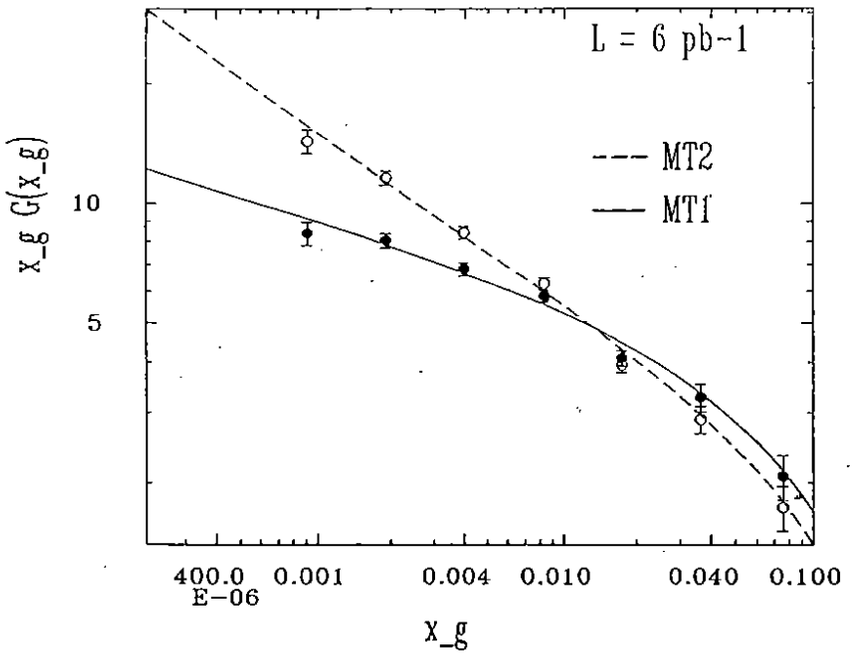

Figure 18

Reconstructed gluon densities from inclusive $D^{*\pm}$ production. The curves show the input gluon functions taken from Morfín and Tung [36]. The error bars include statistical errors for an integrated luminosity of 6 pb^{-1}.

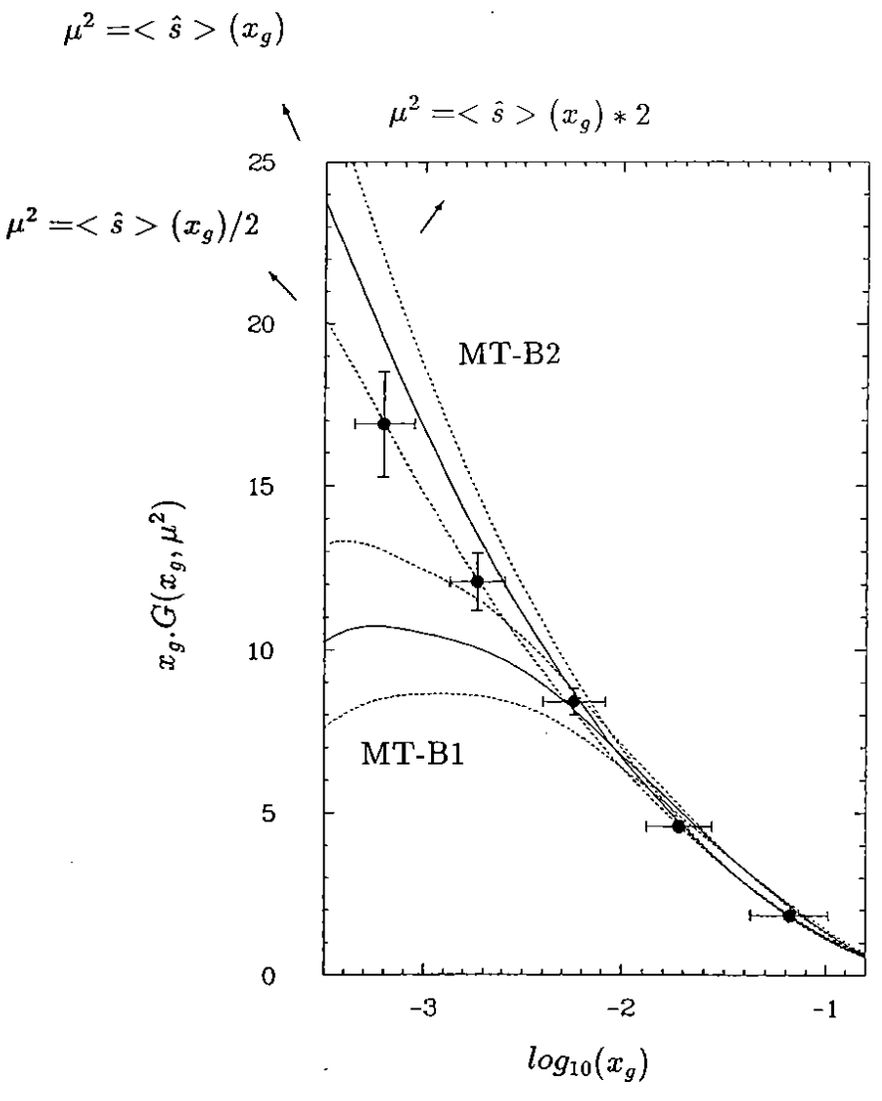

Figure 19

Experimental $G(x_g, \mu^2)$ reconstruction using dileptonic tagged charm events and background. The input gluon density, as shown in the upper solid line, was set B2 of Morfín and Tung. The error bars include statistical as well as systematic errors estimations. The lower solid line represents the prediction of set B1 of Morfín and Tung. The theoretical uncertainty was evaluated by allowing for a relative factor of two in the value of the squared mass scale (dashed lines).